HHS Public Access

Author manuscript

Sci Transl Med. Author manuscript; available in PMC 2021 January 18.

Published in final edited form as:

Sci Transl Med. 2020 July 22; 12(553): . doi:10.1126/scitranslmed.aaw0638.

Apoptosis of hematopoietic progenitor-derived adipose tissue–resident macrophages contributes to insulin resistance after myocardial infarction

Sathish Babu Vasamsetti[1], **Emilie Coppin**[1,2], **Xinyi Zhang**[1,3], **Jonathan Florentin**[1], **Sasha Koul**[4], **Matthias Götberg**[4], **Andrew S. Clugston**[5], **Floyd Thoma**[6], **Sembrat John**[1,7], **Grant C. Bullock**[1], **Dennis Kostka**[5], **Claudette M. Croix St.**[8], **Ansuman Chattopadhyay**[9], **Mauricio Rojas**[1,7], **Suresh R. Mulukutla**[6], **Partha Dutta**[1,6,10,*]

[1]Pittsburgh Heart, Lung, Blood, and Vascular Medicine Institute, University of Pittsburgh Pittsburgh, PA 15213, USA.

[2]Regeneration in Hematopoiesis, Leibniz Institute on Aging- Fritz Lipmann Institute, Jena 07745, Germany.

[3]The Third Xiangya Hospital, Central South University, Changsha, Hunan 410013, China.

[4]Department of Cardiology, Lund University, Skane University Hospital, Lund, 22184, Sweden.

[5]Department of Developmental Biology, University of Pittsburgh, Pittsburgh, PA 15213, USA.

[6]Division of Cardiology, Department of Medicine, University of Pittsburgh, Pittsburgh, PA 15213, USA.

[7]Department of Medicine, Division of Pulmonary, Allergy, and Critical Care Medicine, University of Pittsburgh Medical Center, Pittsburgh, PA 15213, USA.

[8]Department of Cell Biology, University of Pittsburgh, Pittsburgh, PA 15213, USA.

[9]Health Sciences Library System, University of Pittsburgh, PA 15213, USA.

[10]Department of Immunology, University of Pittsburgh, Pittsburgh, PA 15213, USA.

Abstract

[*]Corresponding author. duttapa@pitt.edu.

Author contributions: S.B.V. contributed to the experimental design; conducted experiments involving confocal microscopy, immunoblotting, immunosorbent assays, and GTT; and contributed to data analysis and writing the manuscript. E.C. and J.F. helped conduct the experiments involving cytospin to characterize the morphology of VAT macrophages and analyze publicly available RNA sequencing data. X.Z. performed immunofluorescence microscopy to determine tdTomato expression in VAT macrophages. D.K., A.S.C., and A.C. helped with application of statistical, mathematical, computational, or other formal techniques to analyze or synthesize the study data presented in Fig. 3B and fig. S3C. S.K. and M.G., and S.R.M. and F.T. extracted and analyzed patients' data from SWEDEHEART and UPMC registers, respectively. M.R. and J.S. provided omental adipose tissue from deceased donors. G.C.B. helped in characterizing the morphologies of the VAT macrophage subsets. C.M.S.C. helped with designing the intravital microscopy imaging experiments. P.D. was involved in designing research studies, conducting experiments, acquiring and analyzing data, and writing the manuscript.

Competing interests: The authors declare that they have no competing interests.

Data and materials availability: All data associated with this study are present in the paper or the Supplementary Materials. RNAseq data from this study are available in the GEO database under accession GSE118226. Primary data are available in data file S1.

SUPPLEMENTARY MATERIALS

stm.sciencemag.org/cgi/content/full/12/553/eaaw0638/DC1

Patients with insulin resistance have high risk of cardiovascular disease such as myocardial infarction (MI). However, it is not known whether MI can initiate or aggravate insulin resistance. We observed that patients with ST-elevation MI and mice with MI had de novo hyperglycemia and features of insulin resistance, respectively. In mouse models of both myocardial and skeletal muscle injury, we observed that the number of visceral adipose tissue (VAT)–resident macrophages decreased because of apoptosis after these distant organ injuries. Patients displayed a similar decrease in VAT-resident macrophage numbers and developed systemic insulin resistance after ST-elevation MI. Loss of VAT-resident macrophages after MI injury led to systemic insulin resistance in non-diabetic mice. Danger signaling–associated protein high mobility group box 1 was released by the dead myocardium after MI in rodents and triggered macrophage apoptosis via Toll-like receptor 4. The VAT-resident macrophage population in the steady state in mice was transcriptomically distinct from macrophages in the brain, skin, kidney, bone marrow, lungs, and liver and was derived from hematopoietic progenitor cells just after birth. Mechanistically, VAT-resident macrophage apoptosis and de novo insulin resistance in mouse models of MI were linked to diminished concentrations of macrophage colony-stimulating factor and adiponectin. Collectively, these findings demonstrate a previously unappreciated role of adipose tissue–resident macrophages in sensing remote organ injury and promoting MI pathogenesis.

INTRODUCTION

Tissue-resident macrophages play a crucial role in organ function, tissue homeostasis, and infection and injury. For example, deficiency of alveolar macrophages leads to pulmonary alveolar proteinosis (1), and resident macrophages in pancreatic islets have been shown to initiate autoimmunity in type 1 diabetes (2). Furthermore, tissue macrophages also mediate organ regeneration after tissue injury (3–5). Interleukin-4 (IL-4) receptor signaling in dermal macrophages assembles collagen fibrils during skin repair (6). Tissue-resident macrophages increase the expression of the receptor for apoptotic cell recognition after tissue injury for the clearance of apoptotic bodies (7). These studies demonstrate that macrophages can respond to the alteration of tissue microenvironment due to a local injury. However, how tissue-resident macrophages respond to a distant organ injury is understudied.

The hypothesis that tissue-resident macrophages are maintained by a constant supply of monocytes has been challenged by recent studies showing that most tissue-resident macrophages can sustain by self-renewal (8, 9). The current paradigm is that, with the exception of intestinal macrophages (10), most tissue-resident macrophages arise during successive waves of hematopoiesis in embryo (11, 12). Genetic fate-mapping experiments revealed that Kupffer cells and alveolar, splenic, and peritoneal macrophages are established before birth and maintain themselves without being replenished by blood monocytes (13). Although intestinal macrophages are considered to be blood monocyte–derived, a subset of these macrophages expressing Tim-4 and CD4 develop prenatally and can self-renew without monocytes (14). *Csf1r*$^{+}$ erythromyeloid progenitors independent of Myb (15), a transcription factor required for hematopoietic stem cell development, originate from the yolk sac and fetal liver. These progenitors seed in different organs and differentiate into macrophages before birth (16, 17). A recent study demonstrated that these progenitors generate pre-macrophages that seed the whole embryo starting from embryonic day 9.5

(E9.5) (17). Egress of macrophage progenitors from the fetal liver is mediated by endothelium-specific plasmalemma vesicle-associated protein (18). Some organs such as the heart (19, 20) and testicles (21) contain heterogeneous macrophage populations that are derived from either embryonic progenitors or blood monocytes. The origin of adipose tissue–resident macrophages is not known despite these macrophages playing a critical role in the steady state and disease (22–27). We set out to understand alterations in adipose tissue–resident macrophage population and insulin resistance after a remote organ injury and to discern the ontogeny of macrophage subsets in visceral adipose tissue (VAT).

RESULTS

Mouse adipose tissue contains two distinct subsets of macrophages with different ontogenies

Although the ontogeny of resident macrophages in different tissues has been studied extensively, the ontogeny of VAT macrophage subsets is not known. To identify macrophage subsets in adipose tissues, we checked the expression of CX_3 chemokine receptor 1 (CX3CR1) and C-C chemokine receptor type 2 (CCR2), which are responsible for myeloid cell recruitment and survival (28, 29), in macrophages present in murine gonadal and mesenteric adipose tissue. To this end, we used CX_3CR1 reporter mice that express green fluorescent protein (GFP) under the CX_3CR1 promoter. On the basis of CX_3CR1 and CCR2 expression, we observed two distinct subsets of macrophages present in the adipose tissue of adult mice: CX_3CR1^{high} $CCR2^{high}$ and CX_3CR1^{low} $CCR2^{low}$ (fig. S1, A to C). To further investigate these macrophage subsets, we generated CX_3 $CR1^{CreER/+}$ $ROSA^{tdTomato/+}$ mice that constitutively expressed yellow fluorescent protein under the CX_3CR1 promoter and tdTomato in CX_3CR1^{+} cells upon tamoxifen injection. The VAT of these mice also contained two distinct subsets of macrophages based on their CX_3CR1 expression (fig. S1D). CX_3CR1^{high} and CX_3CR1^{low} macrophages were $CCR2^{high}$ and $CCR2^{low}$, respectively. Tamoxifen injection selectively induced tdTomato expression in CX_3CR1^{high} macrophages but not in CX_3CR1^{low} macrophages.

Next, to determine the ontogeny of these two macrophage populations, we performed parabiosis between $CX_3CR1^{+/GFP}$ CD45.2 and $CX_3CR1^{+/+}$ CD45.1 mice and analyzed leukocyte chimerism in the blood and adipose tissue in $CX_3CR1^{+/+}$ CD45.1 mice 2 months later. Circulating monocytes and neutrophils exhibited about 30% chimerism (fig. S1E). After adjusting to blood monocyte chimerism, the chimerism in CX_3CR1^{high} $CCR2^{high}$ was about 95%, whereas the chimerism in CX_3CR1^{low} $CCR2^{low}$ macrophages was less than 1% (Fig. 1A). Resident macrophages are slowly replaced by circulating monocytes in some tissues such as the heart (30) and choroid plexus (31). To ascertain whether CX_3CR1^{low} $CCR2^{low}$ macrophages in VAT were progressively replenished by blood monocytes, we analyzed the parabionts at 14 and 30 weeks after parabiosis (Fig. 1B). We found that the chimerism in this macrophage population was still low at these time points. To further evaluate the origin of the VAT macrophage subsets, we injected $CX_3CR1^{CreER/+}$ $ROSA^{tdTomato/+}$ mice with tamoxifen for five consecutive days. Immediately after the last tamoxifen injection, CX_3CR1^{high} macrophages expressed tdTomato (Fig. 1, C and D). However, at weeks 4 and 8 after tamoxifen injection, most of these cells were $tdTomato^{-}$,

indicating that this macrophage subset was short-lived and continuously replaced by blood monocytes. Together, the parabiosis and genetic fate mapping experiments suggest that CX_3CR1^{high} $CCR2^{high}$ macrophages were blood monocyte– derived, whereas CX_3CR1^{low} $CCR2^{low}$ macrophages were tissue resident.

Adipose tissue–resident macrophages are derived from progenitors at birth

To determine the ontogeny of VAT-resident macrophages, we generated Csf1r-mer-cre-mer-tdTomato mice that express tdTomato in $Csf1r^+$ cells upon tamoxifen injection. We injected these mice with tamoxifen at 4 weeks of age and analyzed VAT 12 weeks later (Fig. 2A). Consistent with the notion that microglia can self-renew by local proliferation, we observed almost all microglia-retained tdTomato expression (Fig. 2B). In addition, most VAT-resident macrophages were $tdTomato^+$ at the time of analysis (Fig. 2, B and C). Because tdTomato labeling is permanent, these data indicate that VAT-resident macrophages can self-renew. Next, we enumerated macrophage subsets at different time points and found that the frequency of total VAT macrophages progressively decreased after birth (fig. S2, A and B). At birth (postpartum day 0, P0), most VAT macrophages were CX_3CR1^{high} and only about 1% of macrophages were CX_3CR1^{low} (Fig. 2D and fig. S2C). The proportions of CX_3CR1^{high} VAT macrophages gradually decreased, whereas the frequency of CX_3CR1^{low} macrophages increased as the mice aged. In adult mice (P60), most of VAT-resident macrophages were CX_3CR1^{low}.

On the basis of these observations, we hypothesized that CX_3 $CR1^{high}$ macrophages present at birth differentiate into CX_3CR1^{low} macrophages. To test this, we injected pregnant ROSA-tdTomato mice mated with $CX_3CR1^{CreER/CreER}$ male mice with tamoxifen only before birth on E17 (Fig. 2E). Because about 99% of VAT macrophages were CX_3CR1^{high} at birth, almost all VAT macrophages were labeled with tdTomato at this time. On P14, although most CX_3 $CR1^{high}$ macrophages were $tdTomato^+$, CX_3CR1^{low} macrophages were $tdTomato^-$. These data indicate that CX_3CR1^{low} macrophages were not derived from CX_3CR1^{high} macrophages present at birth. To ascertain whether VAT macrophages are yolk sac progenitor–derived, we injected tamoxifen in pregnant ROSA-tdTomato mice mated with Csf1r-mer-cre-mer male mice on E8.5, when $Csf1r^+$ erythromyeloid progenitors arise in the yolk sac (Fig. 2F) (15). Whereas most microglia were $tdTomato^+$ on P0, most VAT macrophages were $tdTomato^-$, indicating that these macrophages were not derived from yolk sac progenitors. A recent study (17) reported that pre-macrophages ($F4/80^-$ $CD11b^-$ CX_3CR1^+ $CD45^+$ $C\text{-}kit^+$) originated from embryonic erythromyeloid progenitors that seed in different organs on E13 before differentiating into tissue-resident macrophages. In line with this finding, we detected cells phenotypically similar to pre-macrophages in VAT of E13 embryo (fig. S2D).

To understand whether pre-macrophages can differentiate into VAT-resident macrophages, we injected tamoxifen at E13 in ROSA-tdTomato female mice mated with Csf1r-mer-cre-mer male mice (Fig. 2G). We found very few $tdTomato^+$ microglia or VAT macrophages at P0, consistent with the notion that $Csf1r^+$ yolk sac progenitors are not present at E13 (16). Because pre-macrophages present at E13 express CX_3CR1 (17), we injected tamoxifen at E13 in ROSA-tdTomato female mice mated with $CX3CR1^{creER/CreER}$ male mice (Fig. 2H).

Only 18% of VAT-resident macrophages were tdTomato^{+} at P28. These data indicate that most VAT-resident macrophages are not derived from pre-macrophages. It has been reported that bone marrow monocytes at the time of birth can infiltrate into tissue such as the aorta (32) and differentiate into macrophages that can self-renew throughout life.

To investigate whether VAT-resident macrophages are derived from precursors present at birth, we injected Csf1r-mer-cre-mer-ROSA-tdTomato offspring with tamoxifen on P0 and determined tdTomato expression on P14 and P28 (Fig. 2I). Most VAT-resident macrophages were tdTomato^{+} on P14 and P28, indicating that this macrophage subset was derived from cells expressing Csf1r on P0. Because bone marrow myeloid progenitors express Csf1r, we assessed the contribution of hematopoietic progenitors in VAT-resident macrophage ontogeny. To this end, we generated mice expressing tdTomato under Flt3, primarily expressed by hematopoietic progenitor cells, upon tamoxifen injection. These mice were injected with tamoxifen on P0 to label Flt3-cre^{+} cells (Fig. 2J and fig. S2E). Analysis on P28 revealed that most VAT-resident macrophages were tdTomato^{+} whereas microglia were tdTomato^{-}, consistent with the idea that microglia are not derived from hematopoietic progenitors. Last, because CX_3CR1 affects macrophage survival, we assessed whether VAT macrophage development depended on this chemokine receptor. Mice deficient in CX_3CR1 had reduced total numbers of VAT macrophages and CCR2^{high} macrophages on P0 and P14 compared to wild-type control; however, leukocyte and CCR2^{low} macrophage numbers were unchanged (fig. S2, F and G). Collectively, these data indicate that VAT-resident macrophages arise from hematopoietic progenitors at birth.

VAT-resident macrophages express a distinct transcriptome profile

To examine the morphology of VAT macrophage subsets, we sorted these macrophages and blood monocytes. Wright-Giemsa staining and flow cytometry analysis (33) revealed that VAT-resident macrophages (CX_3CR1^{low} CCR2^{low}) were larger than monocyte-derived CX_3CR1^{high} CCR2^{high} macrophages and monocytes (Fig. 3A and fig. S3, A and B). In addition, the number of vacuoles was higher in VAT-resident macrophages compared to monocyte-derived VAT macrophages, which had a morphology similar to blood monocytes. Whole transcriptome analysis revealed that VAT-resident macrophages had a distinct transcriptional profile compared to CX3CR1^{high} CCR2^{high} VAT macrophages and monocytes (Fig. 3, B to D) although these macrophage subsets reside in the same microenvironment. CX3 CR1^{high} CCR2^{high} VAT macrophages had higher expression of genes encoding inflammatory cytokines such as *Il1b*, *Il7*, *Tnfa*, and *Infb1* and chemokines such as *Ccl2* and *Ccl5* (fig. S3, C and D), which act as monocyte chemoattractants; IL-1β and IL-6 are known to exacerbate insulin resistance (34). Arg1 has been reported to be highly expressed by tissue-resident macrophages (7, 35). VAT-resident macrophages were enriched in genes responsible for collagen synthesis and transcription factors involved in tissue-resident macrophage maintenance, such as *Gata6* (36).

Next, we analyzed enriched canonical pathways in the VAT macrophage subsets. These analyses revealed that CX_3 CR1^{high} CCR2^{high} VAT macrophages were enriched for pathways involved in blood cell accumulation, macrophage chemotaxis, inflammatory response, and leukocyte migration (fig. S4, A and B). The VAT macrophage subset had

higher expression of genes that mediate chemotaxis and leukocyte migration, such as *Ccl4*, *Ccl5*, and *Cxcl19*. They were also enriched in inflammatory genes such as *Tnf*, *Il1b*, *Ifnb1*, *Itgav*, and *Spp1*. In aggregate, these data suggest that CX_3 $CR1^{high}$ $CCR2^{high}$ VAT macrophages are more proinflammatory and have higher chemotaxis ability than their CX_3CR1^{low} $CCR2^{low}$ counterparts.

The heart contains ontogenically different macrophage populations. In line with a previous observation (20), we found that the heart has at least three types of macrophages based on MHC class II and CCR2 expression (fig. S5A). A longterm parabiosis experiment revealed that MHC class II^{high} $CCR2^{low}$ and MHC class II^{low} $CCR2^{high}$ macrophages are tissue resident and monocyte-derived, respectively. To ascertain whether cardiac and VAT-resident macrophages express similar transcriptome profiles when compared to their respective monocyte-derived macrophage counterparts, we identified canonical pathways that were enriched in the resident cardiac macrophages compared to monocyte-derived cardiac macrophages. Several of these pathways, such as extracellular matrix and collagen triple helix repeat, were common in VAT-resident macrophages (fig. S5B).

Tissue microenvironments shape the transcriptome profile and phenotype of tissue-resident macrophages (1, 37–40). Because the adipose tissue microenvironment is quite different from that of other solid organs, we hypothesized that VAT macrophages exhibit a different transcriptome profile compared to other tissue-resident mac rophages. To test this hypothesis, we analyzed the transcriptome profiles of microglia, Kupffer cells, and alveolar, kidney, skin, and bone marrow macrophages (17, 41). Principal components analysis (PCA) revealed that bone marrow macrophage gene expression was closer to that of CX_3CR1^{high} $CCR2^{high}$ VAT macrophages than CX_3 $CR1^{low}$ $CCR2^{low}$ VAT macrophages (Fig. 3E). Both subsets of VAT macrophages expressed similar gene signatures compared to the other tissue-resident macrophages (Fig. 3E and fig. S6). We identified 93 genes that were up-regulated only in VAT-resident macrophages compared to the other tissue-resident macrophages (fig. S7A). These genes (fig. S7B) included *Foxo1*, *Foxo3*, *Creb1*, *CD44*, *PI3K*, *Smad3*, and *Retnlb*, all reported to be involved in lipid metabolism and insulin sensitivity (42–46), and were enriched canonical pathways such as sirtuin signaling and ERK/MAPK (extracellular signal–regulated kinase/mitogen-activated protein kinase) signaling (Fig. 3F). In addition, we investigated whether VAT-resident macrophages displayed altered expression of inflammatory and anti-inflammatory genes in acute inflammation such as during myocardial infarction (MI). To this end, we performed RNA sequencing in VAT-resident macrophages isolated from mice with or without MI. Even in the inflammatory milieu after MI, this macrophage population did not show increased inflammatory gene expression (fig. S7C). In aggregate, these data demonstrate that VAT-resident macrophages express a distinctive gene signature.

Acute organ injury induces de novo insulin resistance in patients and mice

Because VAT-resident macrophages are crucial to systemic insulin sensitivity (25, 47, 48), we checked fasting blood glucose concentrations in patients 30 days after ST-elevation MI (STEMI). Most patients had glycosylated hemoglobin A1c of less than 6.5% (average, 5.7%) at admission, indicating that these patients were non-diabetic before MI (Fig. 4A). To

assess whether non-diabetic patients develop hyperglycemia after STEMI, we turned to the University of Pennsylvania Medical Center (UPMC) catheterization laboratory database of patients for whom fasting glucose concentrations were available and normal (102 ± 2 mg/dl) 15 days before STEMI. These patients had elevated fasting blood glucose concentrations (130 ± 9 mg/dl) at an average follow up of 30 days after STEMI (Fig. 4B), above the normal fasting glucose cutoff of 110 mg/dl. About 50% of these patients had increased (162 ± 13 mg/dl) fasting blood glucose concentrations, whereas the other 50% had unchanged blood glucose concentrations (99.86 ± 2.5 mg/dl) (Fig. 4C). There was no notable difference in age, gender, and body mass index, or in use of diabetogenic drugs such as statins and beta blockers that are reported to impair insulin release (49) between these two groups of patients (table S1). These data indicate that a subset of non-diabetic patients develops insulin resistance after STEMI.

To understand the mechanisms of hyperglycemia after an organ damage, we used two different mouse models of acute tissue injury: coronary artery ligation, which is a mouse model of MI, and $BaCl_2$-induced skeletal muscle injury. Glucose tolerance tests (GTTs) in non-diabetic lean C57BL/6 mice fed with a chow diet revealed glucose intolerance at days 7 and 28 after MI (Fig. 4D). Obese C57BL/6 mice fed with a high-fat diet for 4 months exhibited delayed glucose clearance after MI (Fig. 4D), demonstrating that MI increases glucose intolerance in mice with established insulin resistance. Lean mice with MI also had hyperinsulinemia, a feature of insulin resistance (Fig. 4E). Congruently, we observed a substantial decrease in the expression of phosphorylated Akt, important for insulin signaling, in the liver and skeletal muscles (Fig. 4F). Similarly, $BaCl_2$-mediated skeletal muscle injury triggered glucose intolerance in mice (Fig. 4G), although their body weights were similar (Fig. 4H). Together, these data indicate that an acute organ injury induces de novo insulin resistance in humans and mice.

Acute injuries in remote organs trigger loss of VAT-resident macrophages

To investigate the mechanisms of insulin resistance after MI, we initially considered multiple potential factors. High amounts of glucocorticoids (50) and catecholamines (51) released immediately after MI can induce insulin resistance. However, high glucocorticoid concentrations did not persist on days 7 and 28 after MI (fig. S8A), and we did not observe any significant increase in catecholamines at day 7 after MI (fig. S8B). In addition, adipose tissue lipolysis (52) accompanied by body weight loss after MI can cause insulin resistance. Mice lost about 10% of their body weight on day 1 after MI (fig. S8C); however, the initial body weight was restored by day 7 after MI, and amounts of serum-free fatty acids and glycerol, markers of lipolysis, on day 7 after MI were unchanged compared to sham-operated mice. Last, insulin resistance in patients with a large MI can be due to underlying heart failure (53, 54). However, we induced a small MI in our mouse model, which did not induce heart failure at day 28 after MI (fig. S8D).

We previously reported that MI increases the production of inflammatory monocyte development (55–57). In line with these findings, flow cytometry confirmed increased numbers of macrophages, myeloid cells, monocytes, and Ly-$6C^{high}$ monocytes in VAT after MI (Fig. 5A and fig. S9A). To determine the dynamics of the two subsets of VAT

macrophages, we performed serial intravital microscopy in $CX_3CR1^{CreER/+}$ $ROSA^{tdTomato/+}$ mice, using tamoxifen injection in these mice to label CX_3CR1^{high} monocyte-derived macrophages with tdTomato. Consistent with increased inflammation after MI, we found a progressive increase in VAT monocyte-derived macrophages after MI (Fig. 5B and movies S1 and S2). However, the frequency of VAT-resident macrophages gradually declined after MI. Similarly, omental VAT in patients with STEMI harbored increased numbers of $CCR2^{high}$ and decreased numbers of $CCR2^{low}$ macrophages compared to that in control patients (Fig. 5C). Congruently, $BaCl_2$-mediated skeletal muscle injury reduced proportions of VAT-resident macrophages (Fig. 5D). To find the origin of newly developed CX_3CR1^{high} macrophages after MI, we performed parabiosis between $CX_3CR1^{+/GFP}$ CD45.2 and CD45.1 mice. One month after, when blood leukocyte chimerism was stable (fig. S9B), we induced MI by coronary artery ligation in CD45.1 mice (Fig. 5E). Most CX_3CR1^{high} macrophages in VAT were derived from the other parabiont, indicating that newly generated monocytes after MI infiltrated into VAT and differentiated into CX_3 $CR1^{high}$ macrophages.

Distant organ injury induces apoptosis of VAT-resident macrophages

To investigate the mechanisms behind the loss of VAT-resident macrophages after MI, we isolated this macrophage subset from mice with or without MI and performed RNA sequencing. VAT-resident macrophages after MI expressed a distinct transcriptomic profile (Fig. 6A). VAT-resident macrophages after MI expressed 118 differentially expressed genes with a 2 $\log_2$ fold cutoff and false discovery rate (FDR)–adjusted $P < 0.05$ compared to the ones isolated from mice without MI (Fig. 6B). Pathway analysis revealed that 12 functional pathways were up-regulated in VAT-resident macrophages isolated from mice with MI (Fig. 6C). These pathways included apoptosis and necrosis (Fig. 6C and fig. S10, A and B), two major mechanisms of cell death, consistent with the observation that MI triggers the disappearance of VAT-resident macrophages in humans and mice (Fig. 5). Of the 118 differentially expressed genes, 16 genes were involved in cellular apoptosis (Fig. 6, D and E, and fig. S10C). Consistent with these observations, mice after MI harbored higher proportions of caspase-3^+, annexin V^+ PI^-, and $TUNEL^+$ VAT-resident macrophages compared to control mice (Fig. 6F and fig. S10, D and E). VAT-resident macrophages did not increase their expression of proinflammatory genes reported to be up-regulated in cells undergoing necroptosis (fig. S10F) (58). To specifically discern whether VAT-resident macrophages undergo necroptosis after MI, we stained these macrophages with an antibody against phosphorylated mixed lineage kinase domain-like protein (MLKL), a sensitive detector of this cell death pathway (59, 60). We did not detect any change in the frequency of $pMLKL^+$ VAT-resident macrophages (fig. S10G), suggesting that these cells do not undergo necroptosis after MI.

VAT-resident macrophage apoptosis initiates glucose intolerance

To explore the importance of VAT-resident macrophages in glucose homeostasis after MI, we depleted this cell subset by systemic clodronate liposome injection (fig. S11A). Mice with MI had impaired glucose clearance after VAT-resident macrophage depletion (fig. S11A). However, systemic clodronate liposome injection likely depletes other tissue-resident macrophages. To specifically test whether VAT-resident macrophages play a crucial role in post-MI glucose intolerance, we directly injected either clodronate or control liposome in

epididymal adipose tissue, the largest abdominal fat depot in non-obese mice, in C57BL/6 mice before inducing MI. This injection resulted in reduced number of VAT-resident macrophages (fig. S11B); however, the numbers of other tissue-resident macrophages such as microglia and liver, heart, and splenic macrophages were unaltered (fig. S11C). The number of VAT monocyte-derived macrophages did not change, most likely due to their high turnover rate (Fig. 1). Mice injected with clodronate liposome had elevated glucose intolerance after MI as determined by a GTT compared to mice injected with control liposome (fig. S11D).

To specifically test the effect of VAT-resident macrophage apoptosis on glucose intolerance in the setting of MI, we generated mice (*LysM*$^{cre/+}$ *ChR2*$^{fl/fl}$) that express the channelrhodopsin-2 (ChR2) protein in macrophages after exposure to blue light (450 to 490 nm). *Chlamydomonas reinhardtii*–derived ChR2 is composed of a blue light–sensitive domain with an ion channel, providing light-dependent ion transport and membrane potential. Illuminating ChR2-expressing macrophages with blue light leads to photostimulation of action potential firing activity. We surgically exposed epididymal adipose tissue and illuminated it with blue light for 20 min. Prolonged blue light exposure of adipose tissue resulted in increased expression of annexin V and caspase-3, markers of apoptosis, in VAT-resident macrophages in these mice (Fig. 6, G and H). This is consistent with the report that chronic stimulation of the ChR-2 signals by blue light induces apoptotic cell death (61). As expected, annexin V expression in microglia, Kupffer cells, and splenic macrophages was unchanged (fig. S11E). In line with their high apoptosis after blue light exposure, the number of VAT-resident macrophages diminished on day 5 after exposure (Fig. 6I). In contrast, the number of VAT monocyte-derived macrophages was unaltered, possibly due to their high turnover rate. To ascertain the function of VAT-resident macrophages after MI, we induced MI in these mice 1 day after VAT-resident macrophage depletion with blue light. VAT-resident macrophage depletion in *LysM*$^{cre/+}$ *ChR-2*$^{fl/fl}$ mice resulted in delayed glucose clearance compared to *LysM*$^{cre/+}$ *ChR-2*$^{fl/fl}$ mice without blue light exposure and *LysM*$^{+/+}$ *ChR-2*$^{fl/fl}$ mice with blue light exposure (Fig. 6J). *LysM*$^{cre/+}$ *ChR-2*$^{fl/fl}$ mice also had elevated fasting insulin concentrations after blue light exposure compared to the control mice (Fig. 6K). Together, these data strongly suggest that VAT-resident macrophage loss after MI drives glucose intolerance.

Distant organ injury alters hepatic metabolism

Next, we investigated whether MI alters resident macrophages in organs other than VAT and observed an increase in total number of liver macrophages on day 7 after MI (fig. S12A). In contrast to the decreased presence of VAT-resident macrophages, we found increased numbers of Kupffer cells (fig. S12, B and C). Concomitantly, hepatic monocyte-derived macrophage and Ly-6C^{high} monocyte numbers increased after MI. MI did not alter liver gluconeogenesis indicated by a pyruvate tolerance test (fig. S12D). However, lipid metabolism was different in lean and obese mice after MI as demonstrated by increased triglyceride quantity in the liver (fig. S12E). Consistent with this finding, genes involved in lipid metabolism (62) were differentially expressed in the liver after MI (fig. S12, F and G). any changes in body weight (fig. S13F) or lipolysis (fig. S13G) in these mice after MI compared to littermate controls. To compensate for decreased Csf1 concentrations after MI,

we infused mice with Csf1 just after coronary artery ligation. Csf1 supplementation improved glucose tolerance (Fig. 7H) and lowered insulin quantity in the blood after fasting (Fig. 7I) after MI. We previously found that MI increases proinflammatory phenotype of monocytes (55), and it is known that Csf1 increases macrophage differentiation (64), suggesting that Csf1 infusion in mice after MI induces a proinflammatory phenotype in VAT-resident macrophages. In contrast, VAT-resident macrophages isolated from Csf1-treated mice after MI expressed reduced amounts of proinflammatory cytokines such as *Tnfa*, *Il1b*, and *Il6* and augmented amounts of anti-inflammatory cytokine genes such as *Tgfb*, *Il10*, and *Il13* (Fig. 7J and fig. S13H) (55, 57, 65, 66).

To specifically test the role of Csf1r expression in VAT macrophages, we performed adipose tissue transplantation in mice (fig. S13I). $LyM^{cre/+}$ $Csf1r^{fl/fl}$ or $LyM^{+/+}$ $Csf1r^{fl/fl}$ epididymal adipose tissue was transplanted into $LyM^{cre/+}$ $Csf1r^{fl/fl}$ or $LyM^{+/+}$ $Csf1r^{fl/fl}$ mice (Fig. 7K). $LyM^{cre/+}$ $Csf1r^{fl/fl}$ mice lack Csf1r in macrophages. We performed MI surgery in these mice 10 days after the transplantation. On day 20 after adipose tissue transplantation, these mice had viable transplanted tissue (fig. S13J). GTTs on day 7 after MI revealed that, as expected, $LyM^{cre/+}$ $Csf1r^{fl/fl}$ mice transplanted with $LyM^{cre/+}$ $Csf1r^{fl/fl}$ adipose tissue had delayed glucose clearance compared with $LyM^{+/+}$ $Csf1r^{fl/fl}$ mice transplanted with $LyM^{+/+}$ $Csf1r^{fl/fl}$ adipose tissue (Fig. 7K). However, the transplantation of $LysM^{+/+}$ $Csf1r^{fl/fl}$ adipose tissue containing $Csf1r^{+}$ macrophages into $LysM^{cre/+}$ $Csf1r^{fl/fl}$ mice improved glucose tolerance. Collectively, these data indicate that Csf1r expression in VAT macrophages is important for glucose tolerance.

On the basis of the data presented above, Csf1 could potentially be used in patients with MI to reduce insulin resistance. However, several lines of evidence suggest that Csf1 increases atherosclerosis (67), which can lead to MI. In contrast, chronic infusion of Csf1 prevents atherosclerosis (68, 69). It is not known whether shortterm Csf1 treatment after MI, as we performed, affects atherosclerosis. To ascertain this, $Apoe^{-/-}$ mice fed with an atherogenic diet were treated with Csf1 after MI. Four months after Csf1 infusion, $Apoe^{-/-}$ mice had unaltered atherosclerotic plaque size compared to the control group (fig. S14A). However, Csf1 infusion decreased inflammatory cell accumulation in the aorta (fig. S14B) and decreased the expression of genes encoding inflammatory cytokines and proteases (fig. S14C), which are reported to increase plaque vulnerability in patients.

HMGB1 induces macrophage apoptosis

Next, we investigated the long-distance signals that trigger apoptosis in VAT-resident macrophages after MI. Dead cardiomyocytes after MI secrete danger-associated molecular patterns (DAMPs); one of the major DAMPs secreted in high concentrations is high mobility group box 1 (HMGB1) (70–72). To determine whether HMGB1 could induce apoptosis of macrophages, we cultured bone marrow–derived macrophages (BMDMs) with various concentrations of HMGB1. This treatment reduced living BMDMs in cell culture (Fig. 8A). In addition, macrophages underwent apoptosis after HMGB1 treatment. HMGB1 binds to Toll-like receptor 4 (TLR4) and advanced glycation end product receptor (AGER) on macrophages (73). To assess whether HMGB1-induced apoptosis of macrophages is mediated by TLR4 and AGER signaling, we knocked down either *Tlr4* or *Ager* in BMDMs

using small interfering RNA (siRNA) before treating with HMGB1. Both si*Tlr4* and si*Ager* decreased the expression of annexin V, a late apoptosis marker, in BMDMs (Fig. 8B). However, only si*Tlr4* treatment decreased the expression of caspase-3, a marker of early apoptosis (Fig. 8C). To understand the role of TLR4 in VAT-resident macrophage loss and glucose intolerance after MI, we induced MI in $Tlr4^{-/-}$ mice. These mice had improved glucose tolerance (Fig. 8D), and reduced annexin V (Fig. 8E) and caspase-3 staining (Fig. 8F) in VAT-resident macrophages after MI.

Decreased adiponectin concentrations after MI induce glucose intolerance

Acute stress conditions can decrease the systemic adiponectin (74–76) that helps maintain systemic insulin sensitivity. To determine whether MI decreases the amounts of this adipokine, we induced MI in C57BL/6 mice. MI decreased adiponectin content in the serum (Fig. 8G). Because MI also decreased the number of VAT-resident macrophages (Fig. 5), which are crucial for insulin sensitivity (Fig. 6), we hypothesized that VAT-resident macrophages help adiponectin secretion by adipocytes. Consistent with this, we observed that the supplementation of Csf1, which is required for tissue-resident macrophage survival, increased serum adiponectin concentrations after MI (Fig. 8H). To specifically test whether VAT-resident macrophages help adiponectin production, we depleted this macrophage population in $LysM^{cre/+}$ $ChR\text{-}2^{fl/fl}$ mice by blue light exposure. This resulted in decreased serum adiponectin contents (Fig. 8I), indicating a role of VAT-resident macrophages in adiponectin production. To understand the importance of adiponectin in glucose intolerance after MI, we induced coronary ligation in adiponectin-deficient mice. These mice had delayed glucose clearance compared with age-matched control mice (Fig. 8J) and increased fasting insulin concentrations (Fig. 8K) although the body weights were not different in these groups of mice (Fig. 8L). In summary, these data suggest that decreased adiponectin concentrations after MI trigger systemic insulin resistance.

Acute inflammation after trauma (77–79), burn (80, 81), and sepsis (82) induces insulin resistance in patients and animal models. To investigate whether inflammation after MI is a nonspecific response or a pathophysiologic process unique to MI, we compared post-MI inflammation with chronic inflammation mediated by obesity and acute nonsterile lipopolysaccharide (LPS)–mediated inflammation as seen in infection. These two pathological conditions are known to induce insulin resistance (43, 82–84). Mice with MI had a higher number of circulatory monocytes than obese mice (fig. S15A). Unlike in MI, obese mice (fig. S15A) and mice with LPS injection (fig. S15B) had increased lipolysis, as indicated by high contents of serum fatty acids. MI also reduced systemic Csf1 concentrations, resulting in decreased numbers of resident macrophages. In contrast, obesity and LPS injection did not change systemic Csf1 concentrations. These data suggest that inflammation after MI has distinct features, which may ultimately have an etiologic link to post-MI insulin resistance.

DISCUSSION

Tissue-resident macrophages can respond to stimuli such as injury and infection in the local environment where they reside (3, 4). A recent study showed that a distant injury can change

the phenotype and function of a tissue-resident macrophage subset (85). Here, we show that VAT-resident macrophages expressed altered transcriptome profiles and underwent apoptosis after an ischemic injury in the heart, resulting in insulin resistance. Our results suggest that these changes in VAT-resident macrophages were mediated by diminished amounts of Csf1 after MI because Csf1 infusion and transplantation of adipose tissue containing *Csf1r*$^{+/+}$ macrophages restored glucose tolerance. In addition, mice lacking *Csf1* globally and *Csf1r* in macrophages had reduced numbers of VAT-resident macrophages and impaired glucose tolerance. These data may indicate a mechanism of the maintenance of insulin sensitivity by Csf1 signaling in VAT-resident macrophages. Further, our results suggest that HMGB1, secreted by dead cardiomyocytes after MI (70–72), induces VAT-resident macrophage apoptosis (fig. S16). This macrophage subset is critical for insulin sensitizing adiponectin production and maintaining glucose tolerance.

Several reports showed that tissue-resident macrophages exhibit disease-specific transformations. A specific subset of microglia is activated in neurodegenerative and neuroinflammatory diseases (86). In addition, tissue-resident macrophages can modulate disease progression; for example, embryo-derived pancreatic macrophages promote ductal adenocarcinoma (87). Our data suggest that VAT-resident macrophages are crucial to maintaining insulin sensitivity. MI promotes the loss of this macrophage population, which may result in glucose intolerance and insulin resistance.

Tissue-resident macrophages are heterogeneous in phenotype and function. Their function and phenotype depend on the chromatin landscape, which is controlled by the microenvironment they reside in (1). This ultimately induces different tissue-specific transcription factors that collaborate with PU.1 to establish tissue-specific enhancers (39, 40). Fully differentiated tissue-resident macrophages can be reprogrammed when they are transferred to a new microenvironment. For example, lung, spleen, liver, and peritoneal macrophages derived from bone marrow cells, when transferred to new tissue environment, acquired enhancers found in embryonic macrophages in a tissue-specific manner (37). In addition, macrophages from different sources, such as the yolk sac, fetal liver, and bone marrow, when transplanted into the lungs, differentiated into alveolar macrophages that were transcriptionally and functionally similar (38). Consistent with these observations, we found that VAT-resident macrophages expressed a unique transcriptome profile compared to other tissue-resident macrophages such as microglia, Kupffer cells, and skin, kidney, alveolar, and bone marrow macrophages. The present study identified a VAT-resident macrophage-specific gene signature that included *Foxo1*, *Foxo3*, *Creb1*, *CD44*, *PI3K*, *Smad3*, and *Retnlb*, which were reported to be involved in lipid metabolism and insulin sensitivity (42–46). When compared to other tissue-resident macrophages, both VAT macrophage subsets had similar transcriptomic profiles, confirming the effect of the tissue microenvironment on macrophage gene expression. However, when we compared the VAT macrophage subsets, we observed that 320 genes were differentially expressed. This is possibly due to the fact that VAT monocyte-derived macrophages are continuously replaced by blood monocytes. Thus, the VAT microenvironment may not be able to fully reshape the chromatin landscape of this macrophage subset to that of VAT-resident macrophages due to the transient life span of VAT monocyte-derived macrophages.

Another finding of our study is that non-diabetic patients and mice develop insulin resistance after MI. Recent publications suggest that patients with MI exhibit insulin resistance and hyperglycemia (88, 89). However, these studies do not address whether these patients had undiagnosed diabetes before MI. Our data demonstrate that patients who were normoglycemic developed hyperglycemia after STEMI. We confirmed this de novo insulin resistance after MI in lean and obese mice. These data indicate that an acute ischemic injury, such as MI, provokes a unique pathophysiological response. Consistently and unlike MI, obesity and LPS-mediated inflammation, although also capable of inducing insulin resistance, did not alter VAT-resident macrophage numbers and Csf1 concentrations but triggered lipolysis. Furthermore, our results suggest that Csf1 infusion in mice after MI ameliorated insulin resistance. Csf1 supplementation did not augment atherosclerotic plaque size; rather, the treatment decreased inflammatory cytokine and leukocyte contents. However, new studies will be required to ascertain the efficacy of Csf1 to reduce insulin resistance in patients after MI.

The current study has several limitations. We observed impaired glucose clearance and improved glucose tolerance in adiponectin- and *Tlr4*-deficient mice, respectively, after MI. However, these mice are known to have altered glucose clearance when fed with a high-fat diet (90, 91). Thus, the effect of adiponectin and *Tlr4* on MI-induced insulin resistance may not be unique to the pathophysiology of MI. Although our experiments involving clodronate liposome and $LysM^{cre/+}$ $ChR2^{fl/fl}$ mice suggest specific depletion of VAT-resident macrophages, we cannot rule out the effect of nonhematopoietic cells on MI-induced insulin resistance. Furthermore, $Tlr4^{-/-}$ mice exhibited reduced VAT-resident macrophage apoptosis and expedited glucose clearance in a GTT; however, we cannot rule out the effect of Tlr4 expressed by other cell types on glucose intolerance after MI. Adipose tissue–resident macrophage-specific Cre recombinase mice will be required to specifically test the contribution of VAT-resident macrophages and the role of Tlr4 expressed by this macrophage subset in glucose intolerance after MI. In contrast to loss of VAT-resident macrophages, the number of Kupffer cells, which are liver-resident macrophages and crucial to insulin resistance, increased after MI. Future studies are warranted to understand the role of Kupffer cells in post-MI insulin resistance. We found that MI altered hepatic lipid content possibly by increasing hepatic inflammation. However, mechanistic studies will be required to understand the mechanisms of altered hepatic lipid content after MI. Our study did not delineate the roles of other DAMPs, such as S100 proteins, heat shock proteins, and mitochondrial DNA, in VAT-resident macrophage apoptosis after MI. Moreover, the systemic release of DAMPs after MI may lead to secondary organ damage, resulting in insulin resistance. Future studies are warranted to assess the contribution of post-MI organ damage in insulin resistance.

MATERIALS AND METHODS

Study design

This study was performed to understand the mechanisms of insulin resistance after MI. The other objectives of the study were to ascertain how a distant organ injury such as MI affects tissue-resident macrophages and to delineate the role of tissue-resident macrophages in MI

pathogenesis. To investigate the changes in VAT-resident macrophages after a distant injury, we used mouse models of acute MI and $BaCl_2$-induced skeletal muscle injury and studied patients with STEMI. To discern the function of VAT-resident macrophages in MI-induced insulin resistance, we depleted macrophages specifically in VAT using clodronate liposomes and induced apoptosis in VAT-resident macrophages in macrophage-specific optogenetic mice. Mice were glucose intolerant after depletion of VAT-resident macrophages. In addition, we used mice lacking adiponectin and *Tlr4* to study the mechanisms of insulin resistance after MI. All animal experiments were conducted following National Institutes of Health (NIH) guidelines under protocols approved by the Institutional Animal Care and Use Committee of the University of Pittsburgh. We further performed a retrospective study in patients with STEMI ($n = 27$) in UPMC catheterization laboratory database to assess insulin resistance after MI. These patients had normal fasting glucose concentrations 15 days before MI and obtained fasting blood glucose concentrations in the patients at 30 days after STEMI. We also collected and analyzed omental adipose tissue from deceased patients with or without MI. Written informed consent was received from family members of deceased patients before tissue collection for the study.

Sample sizes were determined on the basis of our experience of analyzing inflammatory cells after MI. Experiments were replicated as indicated in the figure legends. Quantitative polymerase chain reaction (qPCR) primer sequences are listed in table S2, and primary data used to generate graphs are reported in data file S1. More methods are available in the Supplementary Materials.

Patient samples

To check fasting blood glucose and glycosylated hemoglobin (HbA1c) concentrations in patients with STEMI, we analyzed data of two different patient records: the SWEDEHEART register ($n = 4455$) and UPMC ($n = 27$) patient records. Patients with HbA1c content less than 6.5% were considered non-diabetic. In UPMC patient records, we identified the non-diabetic patients who had known fasting blood glucose concentrations, on average, 15 days before STEMI and 30 days after STEMI. These studies were approved by the University of Pittsburgh Institutional Review Board (IRB no. PRO18010045 and PRO9020115). Omental adipose tissue was collected from deceased patients with or without MI through UPMC autopsy program in a study approved by the University of Pittsburgh Committee for Oversight of Research and Clinical Training Involving Decedents (CORID no. 724). Written informed consent was received from family members of deceased patients before tissue collection.

Mice

The following C57BL/6 mice were purchased from the Jackson Laboratory: *Apoe*$^{-/-}$ (no. 002052), *Adipoq*$^{-/-}$ (no. 008195), *Csf1r*-mer-cre-mer (no. 019098), *CX*$_3$*CR1*$^{gfp/gfp}$ (no. 005582), *CX*$_3$*CR1*^{creER} (no. 021160), *Ccr2*$^{-/-}$ (no. 004999), C57BL/6 (no. 000664), CD45.1 (no. 002014), *Csf1r*$^{fl/fl}$ (no. 021212), *LyzM*$^{cre/cre}$ (no. 004781), *ChR2*$^{fl/fl}$ (no. 12569), ROSA-tdTomato (no. 007914), *Tlr4*$^{-/-}$ (no. 029015), and *Csf1*$^{-/-}$ (op/op) (no. 000231). All mice were housed at UPMC animal facility in individually ventilated cages. Veterinary care was provided by the Division of Laboratory Animal Resources. All facilities were U.S.

Department of Agriculture–registered, covered under an Assurance with the Office of Lab Animal Welfare of the U.S. Public Health Service, and accredited by the Association for Assessment and Accreditation of Laboratory Animal Care International. All animal experiments were conducted following NIH guidelines under protocols approved by the Institutional Animal care and Use Committee of the University of Pittsburgh. We made all attempts to minimize the number of mice required to complete the experiments outlined, and all surgeries were performed under anesthesia. Before surgery, mice were anesthetized using either isoflurane at a concentration of 2% mixed with oxygen at a flow rate of 2 liters/min or by injecting ketamine (100 mg/kg of body weight) combined with xylazine (10 mg/kg of body weight) intraperitoneally. For analgesia, we injected buprenorphine (0.1 mg/kg of body weight intraperitoneally in a volume of 100 μl of saline) in mice after surgery every 12 hours for 3 days. We used 10- to 16-week-old male and female mice for all experiments. For studying atherosclerosis, $Apoe^{-/-}$ mice (10 to 12 weeks old) were fed with a high-fat diet (42% kcal; Research Diets Inc.) for 4 months before MI induction.

Statistical analysis

Data are represented as means ± SEM. Statistical significance between groups was performed using nonparametric Mann-Whitney test or analysis of variance (ANOVA). $P < 0.05$ was considered statistically significant. For generating heatmaps, we selected genes that have an FDR-corrected P value of less than 0.05 and at least twofold increase in expression. To obtain functional pathways, we used a z score cutoff of 2.0.

Supplementary Material

Refer to Web version on PubMed Central for supplementary material.

Acknowledgments:

We thank J. Valmier for providing $Flt3^{creER}$ mice. Mouse cartoons in Figs. 1, 2, and 5 were obtained with free access from Servier Medical Art (http://servier.com) with licensing under the Creative Commons Attribution 3.0 Unported License (http://creativecommons.org/licenses/by/3.0/). Figure S16 was prepared using BioRender (www.biorender.com). We are thankful to A. Chattopadhyay for guidance in analyzing RNAseq data and determining functional pathways.

Funding: This work was supported by National Institute of Health grants R00HL121076-03 (to P.D.), R01HL143967 (to P.D.), and R01HL142629 (to P.D.); AHA Transformational Project Award (19TPA34910142 to P.D.); AHA Innovative Project Award (19IPLOI34760566 to P.D.); and ALA Innovation Project Award (IA-629694 to P.D.). We would like to acknowledge the NIH-supported microscopy resources in the Center for Biologic Imaging, specifically the confocal microscope supported by grant number 1S10OD019973-01. S.B.V. was supported by the AHA Postdoctoral Fellowship Award (20POST35210088 to SBV). J.F. was supported by an NIH Institutional T32 training award.

REFERENCES AND NOTES

1. Amit I, Winter DR, Jung S, The role of the local environment and epigenetics in shaping macrophage identity and their effect on tissue homeostasis. Nat. Immunol 17, 18–25 (2016). [PubMed: 26681458]
2. Carrero JA, McCarthy DP, Ferris ST, Wan X, Hu H, Zinselmeyer BH, Vomund AN, Unanue ER, Resident macrophages of pancreatic islets have a seminal role in the initiation of autoimmune diabetes of NOD mice. Proc. Natl. Acad. Sci. U.S.A 114, E10418–E10427 (2017). [PubMed: 29133420]

3. Aurora AB, Porrello ER, Tan W, Mahmoud AI, Hill JA, Bassel-Duby R, Sadek HA, Olson EN, Macrophages are required for neonatal heart regeneration. J. Clin. Invest 124, 1382–1392 (2014). [PubMed: 24569380]
4. Godwin JW, Pinto AR, Rosenthal NA, Macrophages are required for adult salamander limb regeneration. Proc. Natl. Acad. Sci. U.S.A 110, 9415–9420 (2013). [PubMed: 23690624]
5. Kolter J, Feuerstein R, Zeis P, Hagemeyer N, Paterson N, d'Errico P, Baasch S, Amann L, Masuda T, Lösslein A, Gharun K, Meyer-Luehmann M, Waskow C, Franzke CW, Grün D, Lämmermann T, Prinz M, Henneke P, A subset of skin macrophages contributes to the surveillance and regeneration of local nerves. Immunity 50, 1482–1497.e7 (2019). [PubMed: 31201094]
6. Knipper JA, Willenborg S, Brinckmann J, Bloch W, Maaß T, Wagener R, Krieg T, Sutherland T, Munitz A, Rothenberg ME, Niehoff A, Richardson R, Hammerschmidt M, Allen JE, Eming SA, Interleukin-4 receptor α signaling in myeloid cells controls collagen fibril assembly in skin repair. Immunity 43, 803–816 (2015). [PubMed: 26474656]
7. Roberts AW, Lee BL, Deguine J, John S, Shlomchik MJ, Barton GM, Tissue-resident macrophages are locally programmed for silent clearance of apoptotic cells. Immunity 47, 913–927.e6 (2017). [PubMed: 29150239]
8. Perdiguero EG, Geissmann F, The development and maintenance of resident macrophages. Nat. Immunol 17, 2–8 (2015).
9. Culemann S, Grüneboom A, Nicolás-Ávila JÁ, Weidner D, Lämmle KF, Rothe T, Quintana JA, Kirchner P, Krljanac B, Eberhardt M, Ferrazzi F, Kretzschmar E, Schicht M, Fischer K, Gelse K, Faas M, Pfeifle R, Ackermann JA, Pachowsky M, Renner N, Simon D, Haseloff RF, Ekici AB, Bäuerle T, Blasig IE, Vera J, Voehringer D, Kleyer A, Paulsen F, Schett G, Hidalgo A, Krönke G, Locally renewing resident synovial macrophages provide a protective barrier for the joint. Nature 572, 670–675 (2019). [PubMed: 31391580]
10. Bain CC, Bravo-Blas A, Scott CL, Gomez Perdiguero E, Geissmann F, Henri S, Malissen B, Osborne LC, Artis D, Mowat AM, Constant replenishment from circulating monocytes maintains the macrophage pool in the intestine of adult mice. Nat. Immunol 15, 929–937 (2014). [PubMed: 25151491]
11. Ginhoux F, Guilliams M, Tissue-resident macrophage ontogeny and homeostasis. Immunity 44, 439–449 (2016). [PubMed: 26982352]
12. Ginhoux F, Jung S, Monocytes and macrophages: Developmental pathways and tissue homeostasis. Nat. Rev. Immunol 14, 392–404 (2014). [PubMed: 24854589]
13. Yona S, Kim K-W, Wolf Y, Mildner A, Varol D, Breker M, Strauss-Ayali D, Viukov S, Guilliams M, Misharin A, Hume DA, Perlman H, Malissen B, Zelzer E, Jung S, Fate mapping reveals origins and dynamics of monocytes and tissue macrophages under homeostasis. Immunity 38, 79–91 (2013). [PubMed: 23273845]
14. Shaw TN, Houston SA, Wemyss K, Bridgeman HM, Barbera TA, Zangerle-Murray T, Strangward P, Ridley AJL, Wang P, Tamoutounour S, Allen JE, Konkel JE, Grainger JR, Tissue-resident macrophages in the intestine are long lived and defined by Tim-4 and CD4 expression. J. Exp. Med 215, 1507–1518 (2018). [PubMed: 29789388]
15. Schulz C, Gomez Perdiguero E, Chorro L, Szabo-Rogers H, Cagnard N, Kierdorf K, Prinz M, Wu B, Jacobsen SEW, Pollard JW, Frampton J, Liu KJ, Geissmann F, A lineage of myeloid cells independent of Myb and hematopoietic stem cells. Science 336, 86–90 (2012). [PubMed: 22442384]
16. Gomez Perdiguero E, Klapproth K, Schulz C, Busch K, Azzoni E, Crozet L, Garner H, Trouillet C, de Bruijn MF, Geissmann F, Rodewald HR, Tissue-resident macrophages originate from yolk-sac-derived erythro-myeloid progenitors. Nature 518, 547–551 (2015). [PubMed: 25470051]
17. Mass E, Ballesteros I, Farlik M, Halbritter F, Gunther P, Crozet L, Jacome-Galarza CE, Händler K, Klughammer J, Kobayashi Y, Gomez-Perdiguero E, Schultze JL, Beyer M, Bock C, Geissmann F, Specification of tissue-resident macrophages during organogenesis. Science 353, aaf4238 (2016). [PubMed: 27492475]
18. Rantakari P, Jäppinen N, Lokka E, Mokkala E, Gerke H, Peuhu E, Ivaska J, Elima K, Auvinen K, Salmi M, Fetal liver endothelium regulates the seeding of tissue-resident macrophages. Nature 538, 392–396 (2016). [PubMed: 27732581]

19. Bajpai G, Schneider C, Wong N, Bredemeyer A, Hulsmans M, Nahrendorf M, Epelman S, Kreisel D, Liu Y, Itoh A, Shankar TS, Selzman CH, Drakos SG, Lavine KJ, The human heart contains distinct macrophage subsets with divergent origins and functions. Nat. Med 24, 1234–1245 (2018). [PubMed: 29892064]
20. Epelman S, Lavine KJ, Beaudin AE, Sojka DK, Carrero JA, Calderon B, Brija T, Gautier EL, Ivanov S, Satpathy AT, Schilling JD, Schwendener R, Sergin I, Razani B, Forsberg EC, Yokoyama WM, Unanue ER, Colonna M, Randolph GJ, Mann DL, Embryonic and adult-derived resident cardiac macrophages are maintained through distinct mechanisms at steady state and during inflammation. Immunity 40, 91–104 (2014). [PubMed: 24439267]
21. Mossadegh-Keller N, Gentek R, Gimenez G, Bigot S, Mailfert S, Sieweke MH, Developmental origin and maintenance of distinct testicular macrophage populations. J. Exp. Med 214, 2829–2841 (2017). [PubMed: 28784628]
22. McNelis JC, Olefsky JM, Macrophages, immunity, and metabolic disease. Immunity 41, 36–48 (2014). [PubMed: 25035952]
23. Nagareddy PR, Kraakman M, Masters SL, Stirzaker RA, Gorman DJ, Grant RW, Dragoljevic D, Hong ES, Abdel-Latif A, Smyth SS, Choi SH, Korner J, Bornfeldt KE, Fisher EA, Dixit VD, Tall AR, Goldberg IJ, Murphy AJ, Adipose tissue macrophages promote myelopoiesis and monocytosis in obesity. Cell Metab. 19, 821–835 (2014). [PubMed: 24807222]
24. Nguyen KD, Qiu Y, Cui X, Goh YP, Mwangi J, David T, Mukundan L, Brombacher F, Locksley RM, Chawla A, Alternatively activated macrophages produce catecholamines to sustain adaptive thermogenesis. Nature 480, 104–108 (2011). [PubMed: 22101429]
25. Weisberg SP, McCann D, Desai M, Rosenbaum M, Leibel RL, Ferrante AW Jr., Obesity is associated with macrophage accumulation in adipose tissue. J. Clin. Invest 112, 1796–1808 (2003). [PubMed: 14679176]
26. Jaitin DA, Adlung L, Thaiss CA, Weiner A, Li B, Descamps H, Lundgren P, Bleriot C, Liu Z, Deczkowska A, Keren-Shaul H, David E, Zmora N, Eldar SM, Lubezky N, Shibolet O, Hill DA, Lazar MA, Colonna M, Ginhoux F, Shapiro H, Elinav E, Amit I, Lipid-associated macrophages control metabolic homeostasis in a Trem2-dependent manner. Cell 178, 686–698.e14 (2019). [PubMed: 31257031]
27. Silva HM, Báfica A, Rodrigues-Luiz GF, Chi J, d'Emery Alves Santos P, Reis BS, Hoytema van Konijnenburg DP, Crane A, Arifa RDN, Martin P, Mendes DAGB, Mansur DS, Torres VJ, Cadwell K, Cohen P, Mucida D, Lafaille JJ, Vasculatureassociated fat macrophages readily adapt to inflammatory and metabolic challenges. J. Exp. Med 216, 786–806 (2019). [PubMed: 30862706]
28. Shi C, Jia T, Mendez-Ferrer S, Hohl TM, Serbina NV, Lipuma L, Leiner I, Li MO, Frenette PS, Pamer EG, Bone marrow mesenchymal stem and progenitor cells induce monocyte emigration in response to circulating toll-like receptor ligands. Immunity 34, 590–601 (2011). [PubMed: 21458307]
29. Tsou C-L, Peters W, Si Y, Slaymaker S, Aslanian AM, Weisberg SP, Mack M, Charo IF, Critical roles for CCR2 and MCP-3 in monocyte mobilization from bone marrow and recruitment to inflammatory sites. J. Clin. Invest 117, 902–909 (2007). [PubMed: 17364026]
30. Molawi K, Wolf Y, Kandalla PK, Favret J, Hagemeyer N, Frenzel K, Pinto AR, Klapproth K, Henri S, Malissen B, Rodewald H-R, Rosenthal NA, Bajenoff M, Prinz M, Jung S, Sieweke MH, Progressive replacement of embryo-derived cardiac macrophages with age. J. Exp. Med 211, 2151–2158 (2014). [PubMed: 25245760]
31. Goldmann T, Wieghofer P, Jordão MJC, Prutek F, Hagemeyer N, Frenzel K, Amann L, Staszewski O, Kierdorf K, Krueger M, Locatelli G, Hochgerner H, Zeiser R, Epelman S, Geissmann F, Priller J, Rossi FMV, Bechmann I, Kerschensteiner M, Linnarsson S, Jung S, Prinz M, Origin, fate and dynamics of macrophages at central nervous system interfaces. Nat. Immunol 17, 797–805 (2016). [PubMed: 27135602]
32. Ensan S, Li A, Besla R, Degousee N, Cosme J, Roufaiel M, Shikatani EA, El-Maklizi M, Williams JW, Robins L, Li C, Lewis B, Yun TJ, Lee JS, Wieghofer P, Khattar R, Farrokhi K, Byrne J, Ouzounian M, Zavitz CCJ, Levy GA, Bauer CMT, Libby P, Husain M, Swirski FK, Cheong C, Prinz M, Hilgendorf I, Randolph GJ, Epelman S, Gramolini AO, Cybulsky MI, Rubin BB, Robbins CS, Self-renewing resident arterial macrophages arise from embryonic CX_3CR1^+

precursors and circulating monocytes immediately after birth. Nat. Immunol 17, 159–168 (2016). [PubMed: 26642357]

33. Vasamsetti SB, Florentin J, Coppin E, Stiekema LCA, Zheng KH, Nisar MU, Sembrat J, Levinthal DJ, Rojas M, Stroes ESG, Kim K, Dutta P, Sympathetic neuronal activation triggers myeloid progenitor proliferation and differentiation. Immunity 49, 93–106.e7 (2018). [PubMed: 29958804]
34. Kurauti MA, Costa-Júnior JM, Ferreira SM, Santos GJ, Sponton CHG, Carneiro EM, Telles GD, Chacon-Mikahil MPT, Cavaglieri CR, Rezende LF, Boschero AC, Interleukin-6 increases the expression and activity of insulin-degrading enzyme. Sci. Rep 7, 46750 (2017). [PubMed: 28429777]
35. Rõszer T, Understanding the mysterious M2 macrophage through activation markers and effector mechanisms. Mediators Inflamm. 2015, 816460 (2015). [PubMed: 26089604]
36. Gautier EL, Ivanov S, Williams JW, Huang SC-C, Marcelin G, Fairfax K, Wang PL, Francis JS, Leone P, Wilson DB, Artyomov MN, Pearce EJ, Randolph GJ, Gata6 regulates aspartoacylase expression in resident peritoneal macrophages and controls their survival. J. Exp. Med 211, 1525–1531 (2014). [PubMed: 25024137]
37. Lavin Y, Winter D, Blecher-Gonen R, David E, Keren-Shaul H, Merad M, Jung S, Amit I, Tissue-resident macrophage enhancer landscapes are shaped by the local microenvironment. Cell 159, 1312–1326 (2014). [PubMed: 25480296]
38. van de Laar L, Saelens W, De Prijck S, Martens L, Scott CL, Van Isterdael G, Hoffmann E, Beyaert R, Saeys Y, Lambrecht BN, Guilliams M, Yolk sac macrophages, fetal liver, and adult monocytes can colonize an empty niche and develop into functional tissue-resident macrophages. Immunity 44, 755–768 (2016). [PubMed: 26992565]
39. Gosselin D, Link VM, Romanoski CE, Fonseca GJ, Eichenfield DZ, Spann NJ, Stender JD, Chun HB, Garner H, Geissmann F, Glass CK, Environment drives selection and function of enhancers controlling tissue-specific macrophage identities. Cell 159, 1327–1340 (2014). [PubMed: 25480297]
40. Gosselin D, Skola D, Coufal NG, Holtman IR, Schlachetzki JCM, Sajti E, Jaeger BN, O'Connor C, Fitzpatrick C, Pasillas MP, Pena M, Adair A, Gonda DD, Levy ML, Ransohoff RM, Gage FH, Glass CK, An environment-dependent transcriptional network specifies human microglia identity. Science 356, eaal3222 (2017). [PubMed: 28546318]
41. Takata K, Kozaki T, Lee CZW, Thion MS, Otsuka M, Lim S, Utami KH, Fidan K, Park DS, Malleret B, Chakarov S, See P, Low D, Low G, Garcia-Miralles M, Zeng R, Zhang J, Goh CC, Gul A, Hubert S, Lee B, Chen J, Low I, Shadan NB, Lum J, Wei TS, Mok E, Kawanishi S, Kitamura Y, Larbi A, Poidinger M, Renia L, Ng LG, Wolf Y, Jung S, Önder T, Newell E, Huber T, Ashihara E, Garel S, Pouladi MA, Ginhoux F, Induced-pluripotent-stem-cell-derived primitive macrophages provide a platform for modeling tissue-resident macrophage differentiation and function. Immunity 47, 183–198.e6 (2017). [PubMed: 28723550]
42. Herzig S, Hedrick S, Morantte I, Koo S-H, Galimi F, Montminy M, CREB controls hepatic lipid metabolism through nuclear hormone receptor PPAR-γ. Nature 426, 190–193 (2003). [PubMed: 14614508]
43. McTernan CL, McTernan PG, Harte AL, Levick PL, Barnett AH, Kumar S, Resistin, central obesity, and type 2 diabetes. Lancet 359, 46–47 (2002). [PubMed: 11809189]
44. Seong H-A, Manoharan R, Ha H, Smad proteins differentially regulate obesity-induced glucose and lipid abnormalities and inflammation via class-specific control of AMPK-related kinase MPK38/MELK activity. Cell Death Dis. 9, 471 (2018). [PubMed: 29700281]
45. Sparks JD, Dong HH, FoxO1 and hepatic lipid metabolism. Curr. Opin. Lipidol 20, 217–226 (2009). [PubMed: 21037971]
46. Zhang K, Li L, Qi Y, Zhu X, Gan B, DePinho RA, Averitt T, Guo S, Hepatic suppression of Foxo1 and Foxo3 causes hypoglycemia and hyperlipidemia in mice. Endocrinology 153, 631–646 (2012). [PubMed: 22147007]
47. Boutens L, Stienstra R, Adipose tissue macrophages: Going off track during obesity. Diabetologia 59, 879–894 (2016). [PubMed: 26940592]

48. Weisberg SP, Hunter D, Huber R, Lemieux J, Slaymaker S, Vaddi K, Charo I, Leibel RL, Ferrante AW Jr., CCR2 modulates inflammatory and metabolic effects of high-fat feeding. J. Clin. Invest 116, 115–124 (2006). [PubMed: 16341265]
49. Betteridge DJ, Carmena R, The diabetogenic action of statins—Mechanisms and clinical implications. Nat. Rev. Endocrinol 12, 99–110 (2016). [PubMed: 26668119]
50. Dománski L, Cortisol levels in blood of persons with acute myocardial ischemia and myocardial infarction. Ann. Acad. Med. Stetin 45, 137–155 (1999). [PubMed: 10909487]
51. Little RA, Frayn KN, Randall PE, Stoner HB, Morton C, Yates DW, Laing GS, Plasma catecholamines in the acute phase of the response to myocardial infarction. Arch. Emerg. Med 3, 20–27 (1986). [PubMed: 3524599]
52. Morigny P, Houssier M, Mouisel E, Langin D, Adipocyte lipolysis and insulin resistance. Biochimie 125, 259–266 (2016). [PubMed: 26542285]
53. Aroor AR, Mandavia CH, Sowers JR, Insulin resistance and heart failure: Molecular mechanisms. Heart Fail. Clin 8, 609–617 (2012). [PubMed: 22999243]
54. Ashrafian H, Frenneaux MP, Opie LH, Metabolic mechanisms in heart failure. Circulation 116, 434–448 (2007). [PubMed: 17646594]
55. Dutta P, Courties G, Wei Y, Leuschner F, Gorbatov R, Robbins CS, Iwamoto Y, Thompson B, Carlson AL, Heidt T, Majmudar MD, Lasitschka F, Etzrodt M, Waterman P, Waring MT, Chicoine AT, van der Laan AM, Niessen HWM, Piek JJ, Rubin BB, Butany J, Stone JR, Katus HA, Murphy SA, Morrow DA, Sabatine MS, Vinegoni C, Moskowitz MA, Pittet MJ, Libby P, Lin CP, Swirski FK, Weissleder R, Nahrendorf M, Myocardial infarction accelerates atherosclerosis. Nature 487, 325–329 (2012). [PubMed: 22763456]
56. Dutta P, Sager HB, Stengel KR, Naxerova K, Courties G, Saez B, Silberstein L, Heidt T, Sebas M, Sun Y, Wojtkiewicz G, Feruglio PF, King K, Baker JN, van der Laan AM, Borodovsky A, Fitzgerald K, Hulsmans M, Hoyer F, Iwamoto Y, Vinegoni C, Brown D, Di Carli M, Libby P, Hiebert SW, Scadden DT, Swirski FK, Weissleder R, Nahrendorf M, Myocardial infarction activates CCR2^{+} hematopoietic stem and progenitor cells. Cell Stem Cell 16, 477–487 (2015). [PubMed: 25957903]
57. Leuschner F, Dutta P, Gorbatov R, Novobrantseva TI, Donahoe JS, Courties G, Lee KM, Kim JI, Markmann JF, Marinelli B, Panizzi P, Lee WW, Iwamoto Y, Milstein S, Epstein-Barash H, Cantley W, Wong J, Cortez-Retamozo V, Newton A, Love K, Libby P, Pittet MJ, Swirski FK, Koteliansky V, Langer R, Weissleder R, Anderson DG, Nahrendorf M, Therapeutic siRNA silencing in inflammatory monocytes in mice. Nat. Biotechnol 29, 1005–1010 (2011). [PubMed: 21983520]
58. Zhu K, Liang W, Ma Z, Xu D, Cao S, Lu X, Liu N, Shan B, Qian L, Yuan J, Necroptosis promotes cell-autonomous activation of proinflammatory cytokine gene expression. Cell Death Dis. 9, 500 (2018). [PubMed: 29703889]
59. Galluzzi L, Kroemer G, Necroptosis: A specialized pathway of programmed necrosis. Cell 135, 1161–1163 (2008). [PubMed: 19109884]
60. Shlomovitz I, Zargarian S, Erlich Z, Edry-Botzer L, Gerlic M, Distinguishing necroptosis from apoptosis. Methods Mol. Biol 1857, 35–51 (2018). [PubMed: 30136228]
61. Perny M, Muri L, Dawson H, Kleinlogel S, Chronic activation of the D156A point mutant of Channelrhodopsin-2 signals apoptotic cell death: The good and the bad. Cell Death Dis. 7, e2447 (2016). [PubMed: 27809305]
62. Liu Q, Yuan B, Lo KA, Patterson HC, Sun Y, Lodish HF, Adiponectin regulates expression of hepatic genes critical for glucose and lipid metabolism. Proc. Natl. Acad. Sci. U.S.A 109, 14568–14573 (2012). [PubMed: 22904186]
63. Davies LC, Rosas M, Jenkins SJ, Liao C-T, Scurr MJ, Brombacher F, Fraser DJ, Allen JE, Jones SA, Taylor PR, Distinct bone marrow-derived and tissue-resident macrophage lineages proliferate at key stages during inflammation. Nat. Commun 4, 1886 (2013). [PubMed: 23695680]
64. Hashimoto D, Chow A, Greter M, Saenger Y, Kwan W-H, Leboeuf M, Ginhoux F, Ochando JC, Kunisaki Y, van Rooijen N, Liu C, Teshima T, Heeger PS, Stanley ER, Frenette PS, Merad M, Pretransplant CSF-1 therapy expands recipient macrophages and ameliorates GVHD after allogeneic hematopoietic cell transplantation. J. Exp. Med 208, 1069–1082 (2011). [PubMed: 21536742]

65. Dutta P, Hoyer FF, Grigoryeva LS, Sager HB, Leuschner F, Courties G, Borodovsky A, Novobrantseva T, Ruda VM, Fitzgerald K, Iwamoto Y, Wojtkiewicz G, Sun Y, Da Silva N, Libby P, Anderson DG, Swirski FK, Weissleder R, Nahrendorf M, Macrophages retain hematopoietic stem cells in the spleen via VCAM-1. J. Exp. Med 212, 497–512 (2015). [PubMed: 25800955]

66. Dutta P, Nahrendorf M, Monocytes in myocardial infarction. Arterioscler. Thromb. Vasc. Biol 35, 1066–1070 (2015). [PubMed: 25792449]

67. Shaposhnik Z, Wang X, Lusis AJ, Arterial colony stimulating factor-1 influences atherosclerotic lesions by regulating monocyte migration and apoptosis. J. Lipid Res 51, 1962–1970 (2010). [PubMed: 20194110]

68. Inoue I, Inaba T, Motoyoshi K, Harada K, Shimano H, Kawamura M, Gotoda T, Oka T, Shiomi M, Watanabe Y, Tsukada T, Yazaki Y, Takaku F, Yamada N, Macrophage colony stimulating factor prevents the progression of atherosclerosis in Watanabe heritable hyperlipidemic rabbits. Atherosclerosis 93, 245–254 (1992). [PubMed: 1590829]

69. Tojo N, Asakura E, Koyama M, Tanabe T, Nakamura N, Effects of macrophage colony-stimulating factor (M-CSF) on protease production from monocyte, macrophage and foam cell in vitro: A possible mechanism for anti-atherosclerotic effect of M-CSF. Biochim. Biophys. Acta 1452, 275–284 (1999). [PubMed: 10590316]

70. Cirillo P, Giallauria F, Pacileo M, Petrillo G, D'Agostino M, Vigorito C, Chiariello M, Increased high mobility group box-1 protein levels are associated with impaired cardiopulmonary and echocardiographic findings after acute myocardial infarction. J. Card. Fail 15, 362–367 (2009). [PubMed: 19398086]

71. Kohno T, Anzai T, Naito K, Miyasho T, Okamoto M, Yokota H, Yamada S, Maekawa Y, Takahashi T, Yoshikawa T, Ishizaka A, Ogawa S, Role of high-mobility group box 1 protein in post-infarction healing process and left ventricular remodelling. Cardiovasc. Res 81, 565–573 (2009). [PubMed: 18984601]

72. Sørensen MV, Pedersen S, Møgelvang R, Skov-Jensen J, Flyvbjerg A, Plasma high-mobility group box 1 levels predict mortality after ST-segment elevation myocardial infarction. JACC Cardiovasc. Interv 4, 281–286 (2011). [PubMed: 21435605]

73. Andrassy M, Volz HC, Igwe JC, Funke B, Eichberger SN, Kaya Z, Buss S, Autschbach F, Pleger ST, Lukic IK, Bea F, Hardt SE, Humpert PM, Bianchi ME, Mairbaurl H, Nawroth PP, Remppis A, Katus HA, Bierhaus A, High-mobility group box-1 in ischemia-reperfusion injury of the heart. Circulation 117, 3216–3226 (2008). [PubMed: 18574060]

74. Konter JM, Parker JL, Baez E, Li SZ, Ranscht B, Denzel M, Little FF, Nakamura K, Ouchi N, Fine A, Walsh K, Summer RS, Adiponectin attenuates lipopolysaccharide-induced acute lung injury through suppression of endothelial cell activation. J. Immunol 188, 854–863 (2012). [PubMed: 22156343]

75. Shiloah E, Kanety H, Cohen O, Witz S, Buchs A, Pariente C, Rapoport MJ, Acute psychotic stress is associated with decreased adiponectin serum levels. J. Endocrinol. Invest 30, 382–387 (2007). [PubMed: 17598969]

76. Venkatesh B, Hickman I, Nisbet J, Cohen J, Prins J, Changes in serum adiponectin concentrations in critical illness: A preliminary investigation. Crit. Care 13, R105 (2009). [PubMed: 19570238]

77. Li L, Messina JL, Acute insulin resistance following injury. Trends Endocrinol. Metab 20, 429–435 (2009). [PubMed: 19800814]

78. Ma Y, Toth B, Keeton AB, Holland LT, Chaudry IH, Messina JL, Mechanisms of hemorrhage-induced hepatic insulin resistance: Role of tumor necrosis factor-α. Endocrinology 145, 5168–5176 (2004). [PubMed: 15297437]

79. Ma Y, Wang P, Kuebler JF, Chaudry IH, Messina JL, Hemorrhage induces the rapid development of hepatic insulin resistance. Am. J. Physiol. Gastrointest. Liver Physiol 284, G107–G115 (2003). [PubMed: 12388175]

80. Cree MG, Aarsland A, Herndon DN, Wolfe RR, Role of fat metabolism in burn trauma-induced skeletal muscle insulin resistance. Crit. Care Med 35, S476–S483 (2007). [PubMed: 17713396]

81. Xu J, Kim HT, Ma Y, Zhao L, Zhai L, Kokorina N, Wang P, Messina JL, Trauma and hemorrhage-induced acute hepatic insulin resistance: Dominant role of tumor necrosis factor-α. Endocrinology 149, 2369–2382 (2008). [PubMed: 18187553]

82. Hui JM, Sud A, Farrell GC, Bandara P, Byth K, Kench JG, McCaughan GW, George J, Insulin resistance is associated with chronic hepatitis C virus infection and fibrosis progression [corrected]. Gastroenterology 125, 1695–1704 (2003). [PubMed: 14724822]

83. Ma L-J, Mao S-L, Taylor KL, Kanjanabuch T, Guan Y, Zhang Y, Brown NJ, Swift LL, McGuinness OP, Wasserman DH, Vaughan DE, Fogo AB, Prevention of obesity and insulin resistance in mice lacking plasminogen activator inhibitor 1. Diabetes 53, 336–346 (2004). [PubMed: 14747283]

84. Mulligan K, Grunfeld C, Tai VW, Algren H, Pang M, Chernoff DN, Lo JC, Schambelan M, Hyperlipidemia and insulin resistance are induced by protease inhibitors independent of changes in body composition in patients with HIV infection. J. Acquir. Immune Defic. Syndr 23, 35–43 (2000). [PubMed: 10708054]

85. Hoyer FF, Naxerova K, Schloss MJ, Hulsmans M, Nair AV, Dutta P, Calcagno DM, Herisson F, Anzai A, Sun Y, Wojtkiewicz G, Rohde D, Frodermann V, Vandoorne K, Courties G, Iwamoto Y, Garris CS, Williams DL, Breton S, Brown D, Whalen M, Libby P, Pittet MJ, King KR, Weissleder R, Swirski FK, Nahrendorf M, Tissue-specific macrophage responses to remote injury impact the outcome of subsequent local immune challenge. Immunity 51, 899–914.e7 (2019). [PubMed: 31732166]

86. Mrdjen D, Pavlovic A, Hartmann FJ, Schreiner B, Utz SG, Leung BP, Lelios I, Heppner FL, Kipnis J, Merkler D, Greter M, Becher B, High-dimensional single-cell mapping of central nervous system immune cells reveals distinct myeloid subsets in health, aging, and disease. Immunity 48, 380–395.e6 (2018). [PubMed: 29426702]

87. Zhu Y, Herndon JM, Sojka DK, Kim K-W, Knolhoff BL, Zuo C, Cullinan DR, Luo J, Bearden AR, Lavine KJ, Yokoyama WM, Hawkins WG, Fields RC, Randolph GJ, DeNardo DG, Tissue-resident macrophages in pancreatic ductal adenocarcinoma originate from embryonic hematopoiesis and promote tumor progression. Immunity 47, 323–338.e6 (2017). [PubMed: 28813661]

88. Nishio K, Shigemitsu M, Kusuyama T, Fukui T, Kawamura K, Itoh S, Konno N, Katagiri T, Insulin resistance in nondiabetic patients with acute myocardial infarction. Cardiovasc. Revasc. Med 7, 54–60 (2006). [PubMed: 16757401]

89. Reaven G, Calciano A, Cody R, Lucas C, Miller R, Carbohydrate intolerance and hyperlipemia in patients with myocardial infarction without known diabetes mellitus. J. Clin. Endocrinol. Metab 23, 1013–1023 (1963). [PubMed: 14067888]

90. Shi H, Kokoeva MV, Inouye K, Tzameli I, Yin H, Flier JS, TLR4 links innate immunity and fatty acid-induced insulin resistance. J. Clin. Invest 116, 3015–3025 (2006). [PubMed: 17053832]

91. Turer AT, Scherer PE, Adiponectin: Mechanistic insights and clinical implications. Diabetologia 55, 2319–2326 (2012). [PubMed: 22688349]

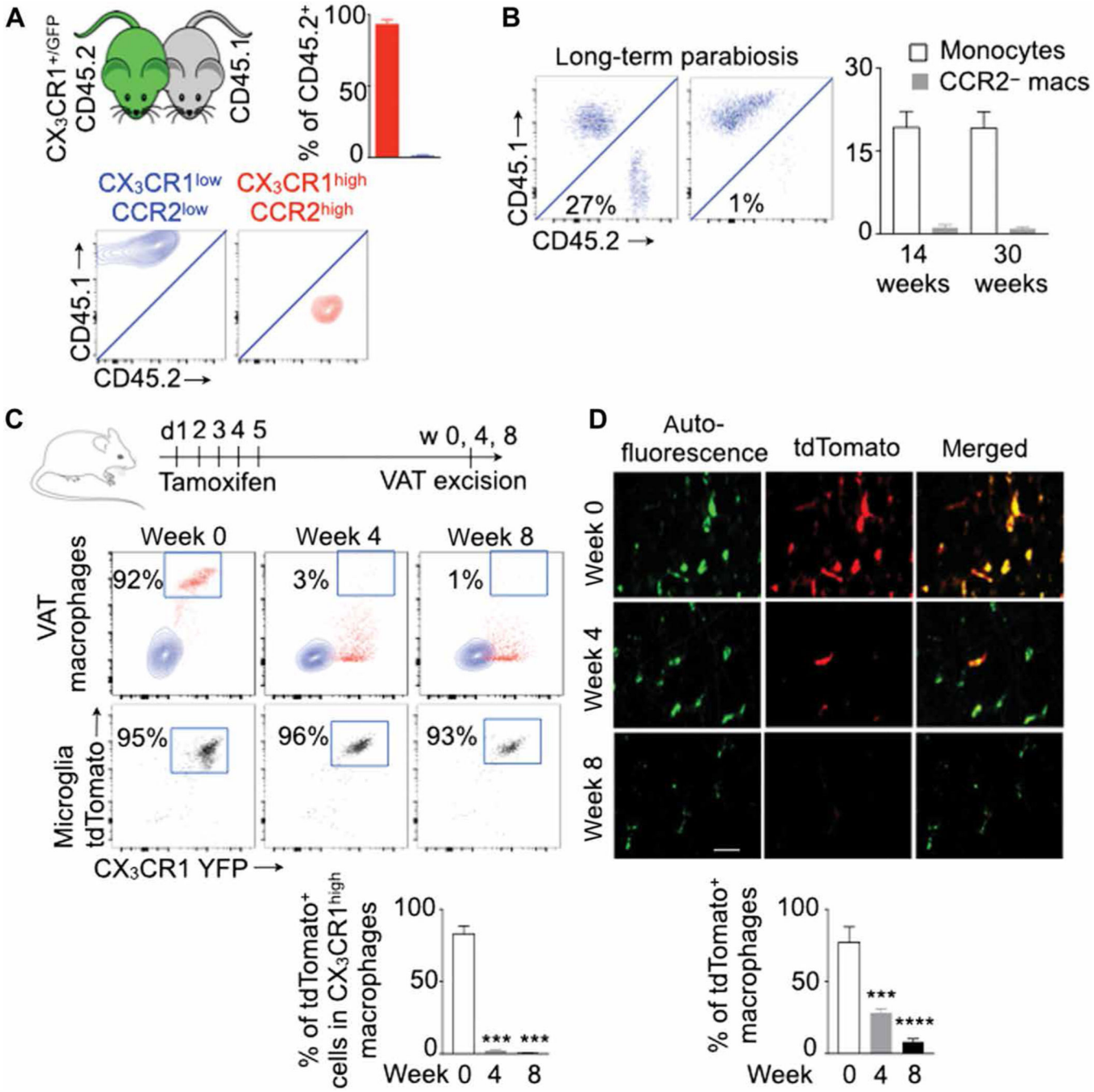

Fig. 1. CX_3CR1^{high} $CCR2^{high}$ and CX_3CR1^{low} $CCR2^{low}$ macrophages in adipose tissue are monocyte-derived and resident macrophages, respectively.

All experiments were performed in lean transgenic mice without MI. (**A**) Parabiosis between wild-type (CD45.1) and $CX_3CR1^{+/GFP}$ (CD45.2) mice was performed, and visceral adipose tissue (VAT) in CD45.1 mice was analyzed for chimerism 2 months after the parabiosis. The chimerism in VAT macrophage subsets was adjusted to that in blood monocytes. $n = 4$ pairs per group. (**B**) Chimerism in blood monocytes and VAT-resident macrophages (macs) was quantified at 14 and 30 weeks after parabiosis. $n = 6$ pairs per group. (**C** and **D**) Genetic fate

mapping in $CX_3CR1^{CreER/+}$ $ROSA^{tdTomato/+}$ mice to test the origin of CX_3CR1^{high} $CCR2^{high}$ macrophages. $TdTomato^+$ (CX_3CR1^{high}) macrophages were quantified at different time points after tamoxifen injection using flow cytometry (C) and confocal microscopy (D). VAT macrophages are autofluorescent (green). Scale bar, 7 μm. $n = 3$ to 11 per group. Data are derived from three independent experiments. Means ± SEM. ***$P < 0.001$ and ****$P < 0.0001$.

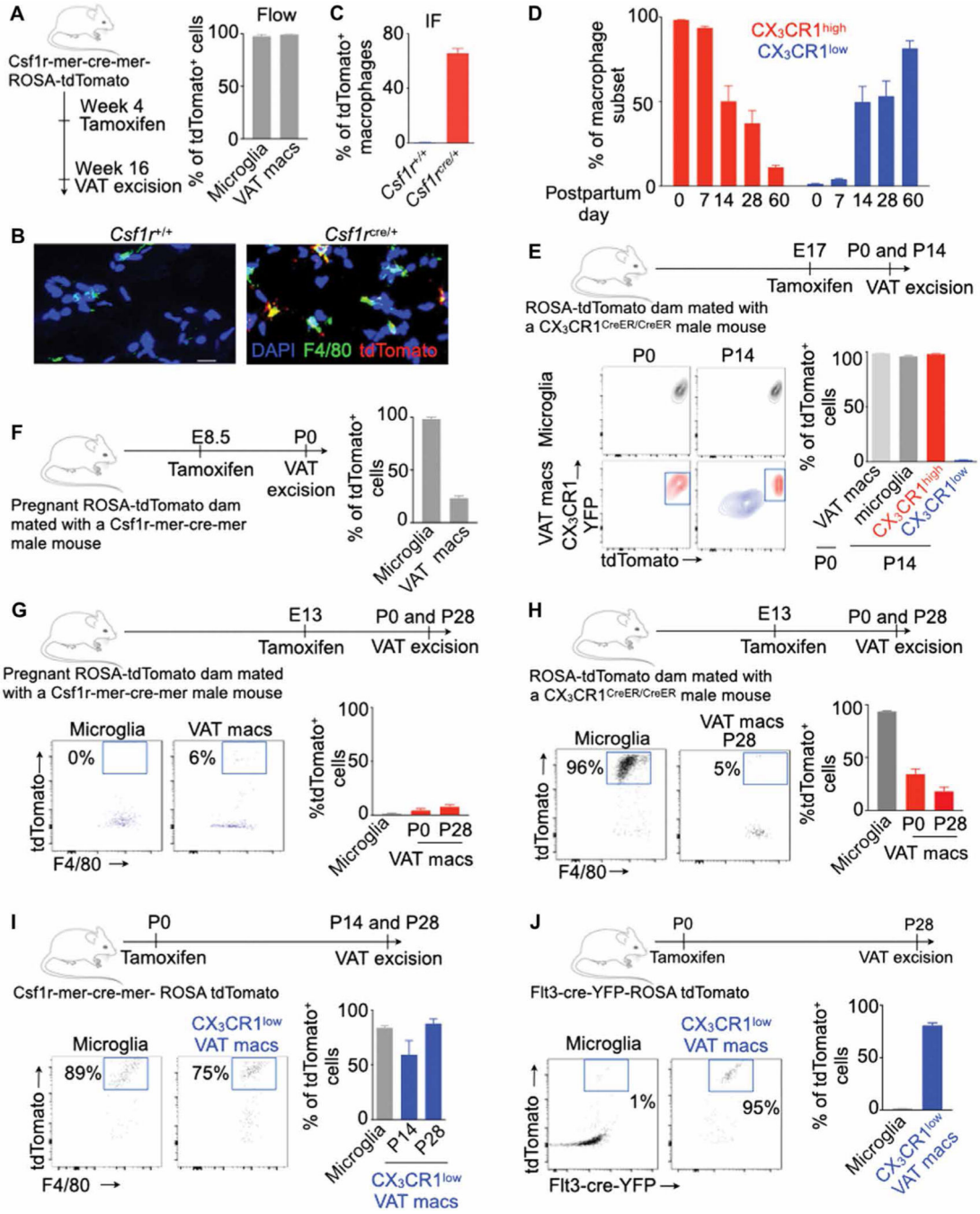

Fig. 2. VAT-resident macrophages are derived from progenitors present at birth.

All experiments were performed in lean transgenic mice without myocardial infarction (MI) at different time points after birth as shown. (**A** to **C**) The frequency of tdTomato^{+} VAT-resident macrophages was quantified using flow cytometry (A) (n = 7 per group) and confocal microscopy (B and C) (n = 3 to 4 per group). Scale bar, 20 μm. (**D**) Frequency of the VAT macrophages at different time points after birth in CX$_3$CR1$^{+/GFP}$ mice. n = 3 to 4 per group. (**E** to **J**) Experimental design and quantification of tdTomato^{+} VAT macrophages labeled by tamoxifen injection in various lineage-tracing mice. n = 3 to 4 per group in (E); n

= 3 per group in (F); n = 5 to 6 per group in (G); n = 5 to 12 per group in (H); n = 4 (P14) and n = 8 (P28) in (I); and n = 3 (microglia) and n = 8 (macrophages) in (J). Tamoxifen was injected in either pregnant dams or offspring, and tdTomato$^+$ VAT-resident macrophages were enumerated by flow cytometry at various time points as shown. Data are from two to three independently performed experiments. IF, immunofluorescence; DAPI, 4′,6-diamidino-2-phenylindole. Means ± SEM.

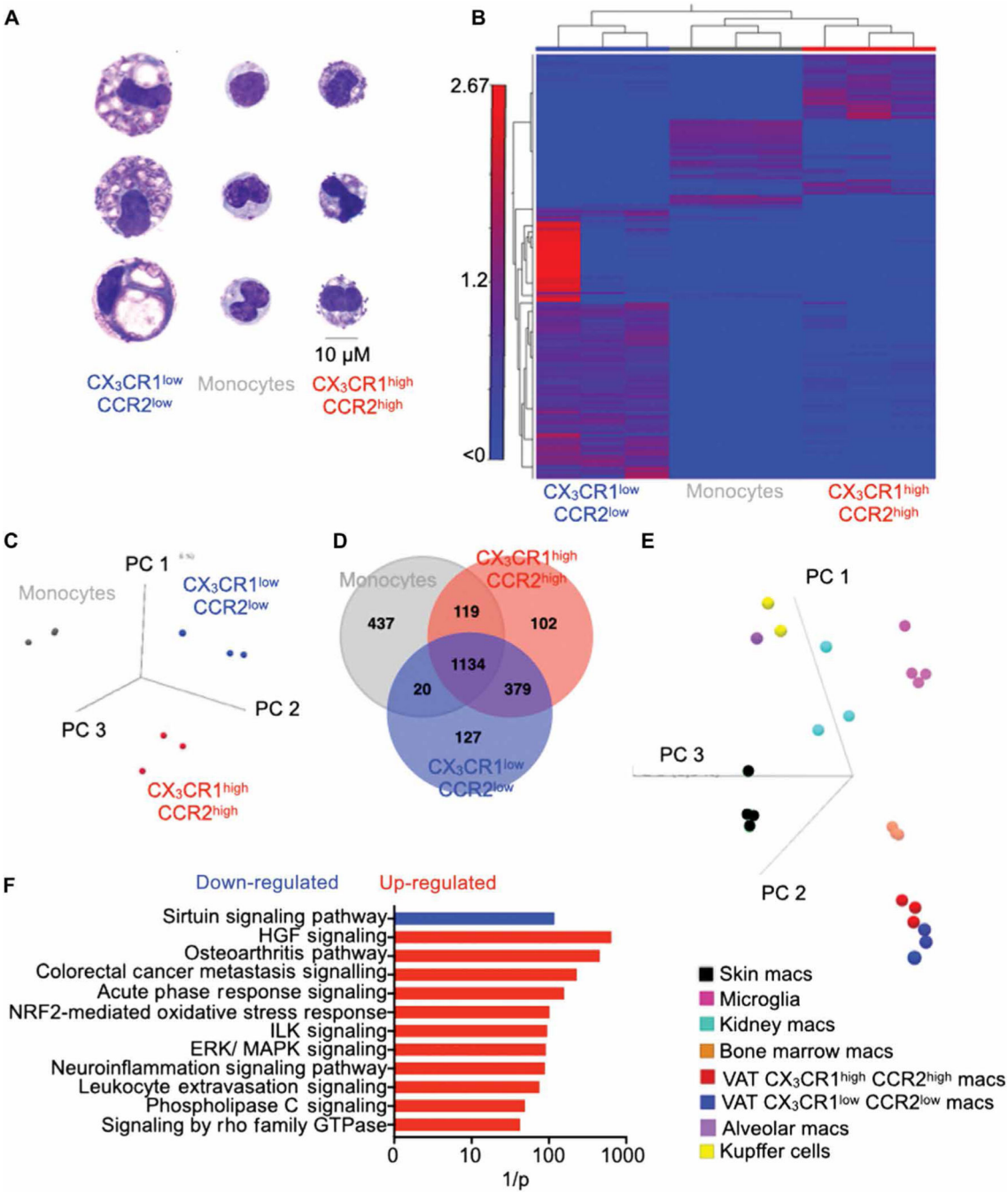

Fig. 3. VAT-resident macrophages exhibit a unique transcriptome profile.

All experiments were performed in lean C57BL/6 mice without MI. (**A**) Assessment of morphology of isolated blood monocytes and VAT macrophages by Wright-Giemsa staining. Scale bar, 10 μm. (**B**) The heatmap displays genes obtained from RNA sequencing analysis with at least twofold difference between the VAT macrophage subsets (FDR < 0.05). Principal components analysis (PCA) (**C**) and a Venn diagram (**D**) showing differentially expressed genes among monocytes and the VAT macrophage subsets. PCA plot (**E**) and bar graph (**F**) compare VAT macrophages to other tissue-resident macrophages. $n = 3$ per group.

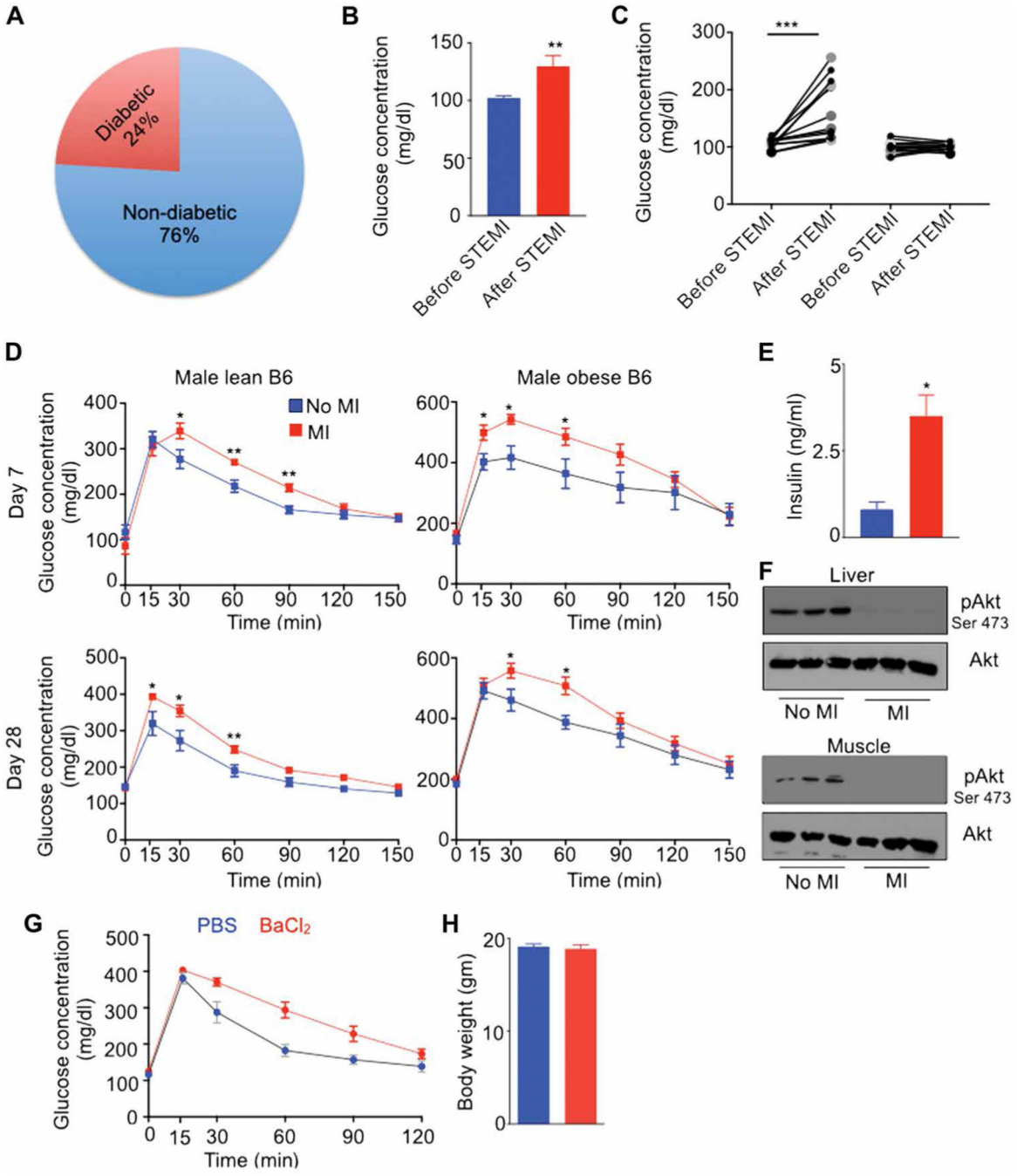

Fig. 4. Acute organ injuries trigger insulin resistance in non-diabetic patients and mice.

(**A**) Distribution of patient groups at admission in patients with ST-elevation MI (STEMI). *n* = 4455. (**B** and **C**) Fasting blood glucose concentrations in non-diabetic patients 15 days (average) before and 30 days after STEMI. *n* = 27 per group. (**D**) Glucose tolerance test (GTT) in lean and obese C57BL/6 mice after MI. Fasting serum insulin concentrations (**E**) and pAkt contents in the liver and skeletal muscle (**F**) in lean C57BL/6 mice at day 7 after MI. *n* = 6 to 7 per group. (**G**) GTT 7 days after $BaCl_2$ injection. Data pooled from two

independently performed experiments. Means ± SEM. *$P < 0.05$, **$P < 0.01$, and ***$P < 0.001$.

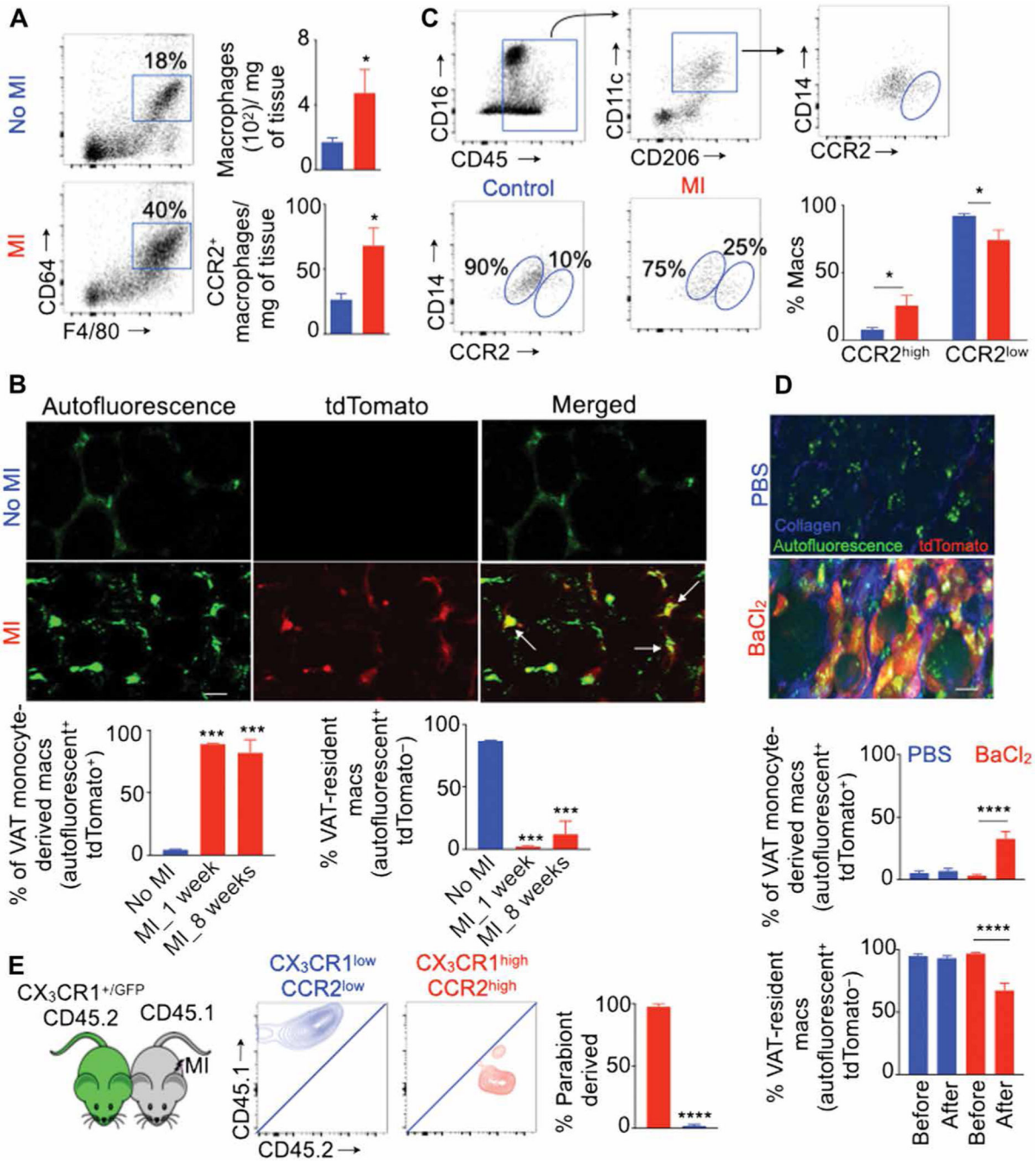

Fig. 5. Acute injuries in distant organs result in a reduction of VAT-resident macrophages.

Quantification of VAT macrophage subsets using flow cytometry in lean C57BL/6 mice on day 7 after MI (n = 3 to 7 per group) (**A**), intravital microscopy in lean $CX_3CR1^{CreER/+}$ $ROSA^{tdTomato/+}$ mice on days 7 and 60 after MI (n = 4 per group) (**B**), and flow cytometry in patients with STEMI (n = 4 to 5 per group) (**C**). Data pooled from three independent experiments. Scale bar, 7 μm. (**D**) Quantification of VAT macrophages after $BaCl_2$-induced skeletal muscle injury in lean $CX_3CR1^{CreER/+}$ $ROSA^{tdTomato/+}$ mice using intravital microscopy. n = 6 per group. Scale bar, 20 μm. (**E**) Chimerism in VAT macrophage subsets

in lean CD45.1^{+} parabiont mice 1 week after MI. $n = 4$ pairs per group. Means ± SEM. *$P <$ 0.05, ***$P < 0.001$, and ****$P < 0.0001$.

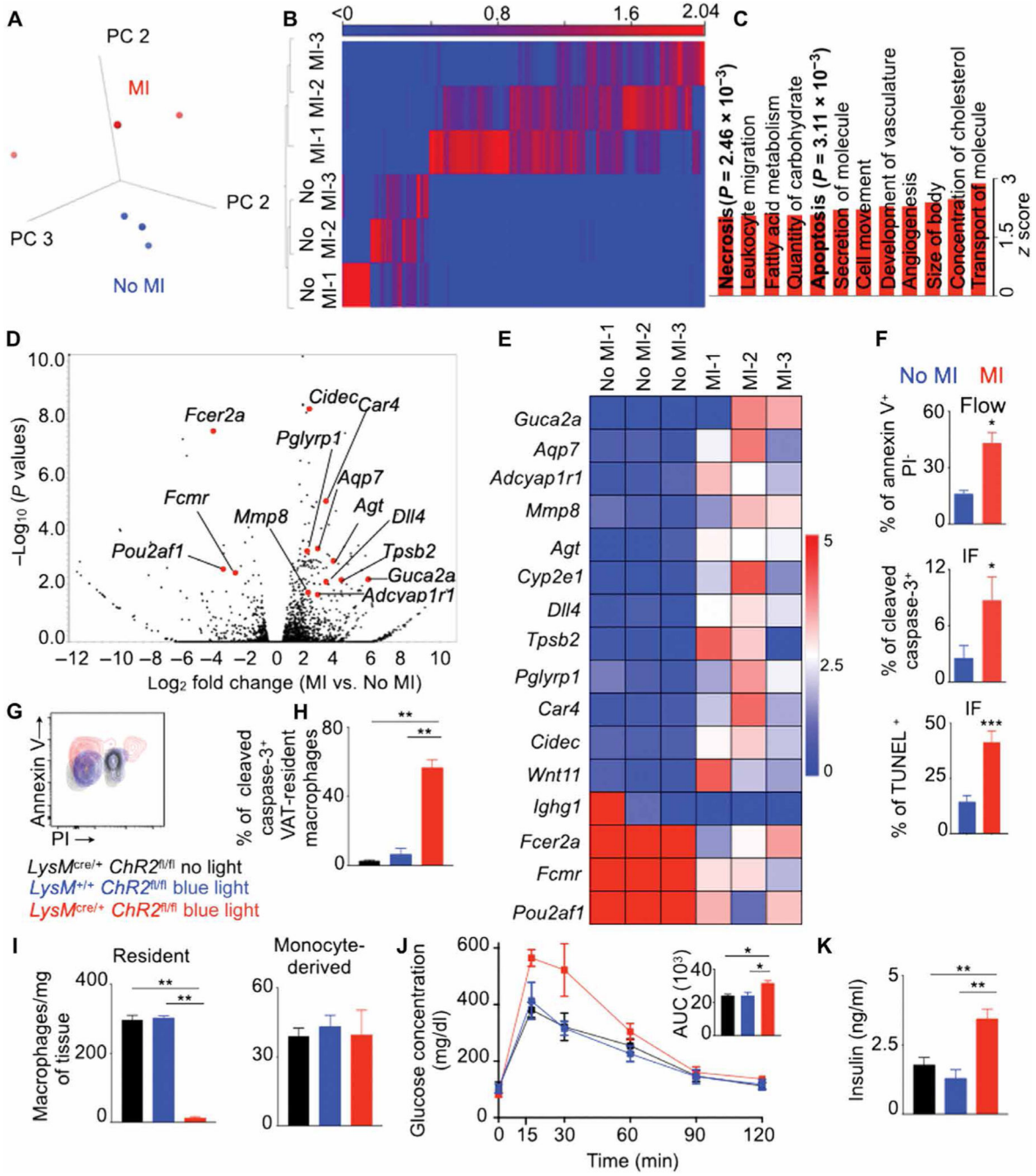

Fig. 6. Apoptosis of VAT-resident macrophages after MI increases glucose intolerance.

Experiments were performed in lean C57BL/6 mice on day 7 after MI. (**A**) PCA of RNA sequencing data comparing the transcriptomic profiles of VAT-resident macrophages isolated from mice with or without MI. (**B**) Differentially expressed genes with a 2 $\log_2$ fold cutoff and FDR < 0.05. (**C**) Functional pathways increased in VAT-resident macrophages in mice with MI. (**D**) Volcano plot and (**E**) heatmap showing genes involved in cellular apoptosis. *n* = 3 for (A) to (E). (**F**) Quantification of annexin V^+ propidium iodide (PI), cleaved caspase-3^+, and $TUNEL^+$ VAT-resident macrophages by flow cytometry and confocal

microscopy. $n = 10$ per group. (**G** to **K**) MI was performed in lean *LysM*$^{cre/+}$ *ChR2*$^{fl/fl}$ and control mice on day 5 after blue light exposure. (G and H) Annexin V and caspase-3 expression in VAT-resident macrophages on day 1 after blue light exposure. (I) Enumeration of VAT-resident and monocyte-derived macrophages on day 5 after blue light exposure. A GTT was performed (J), and serum insulin concentrations were measured (K) in mice 7 days after MI (6 days after blue light exposure). $n = 4$ per group for (G) to (K). AUC, area under the curve. Means ± SEM. $^{*}P < 0.05$, $^{**}P < 0.01$, and $^{***}P < 0.001$.

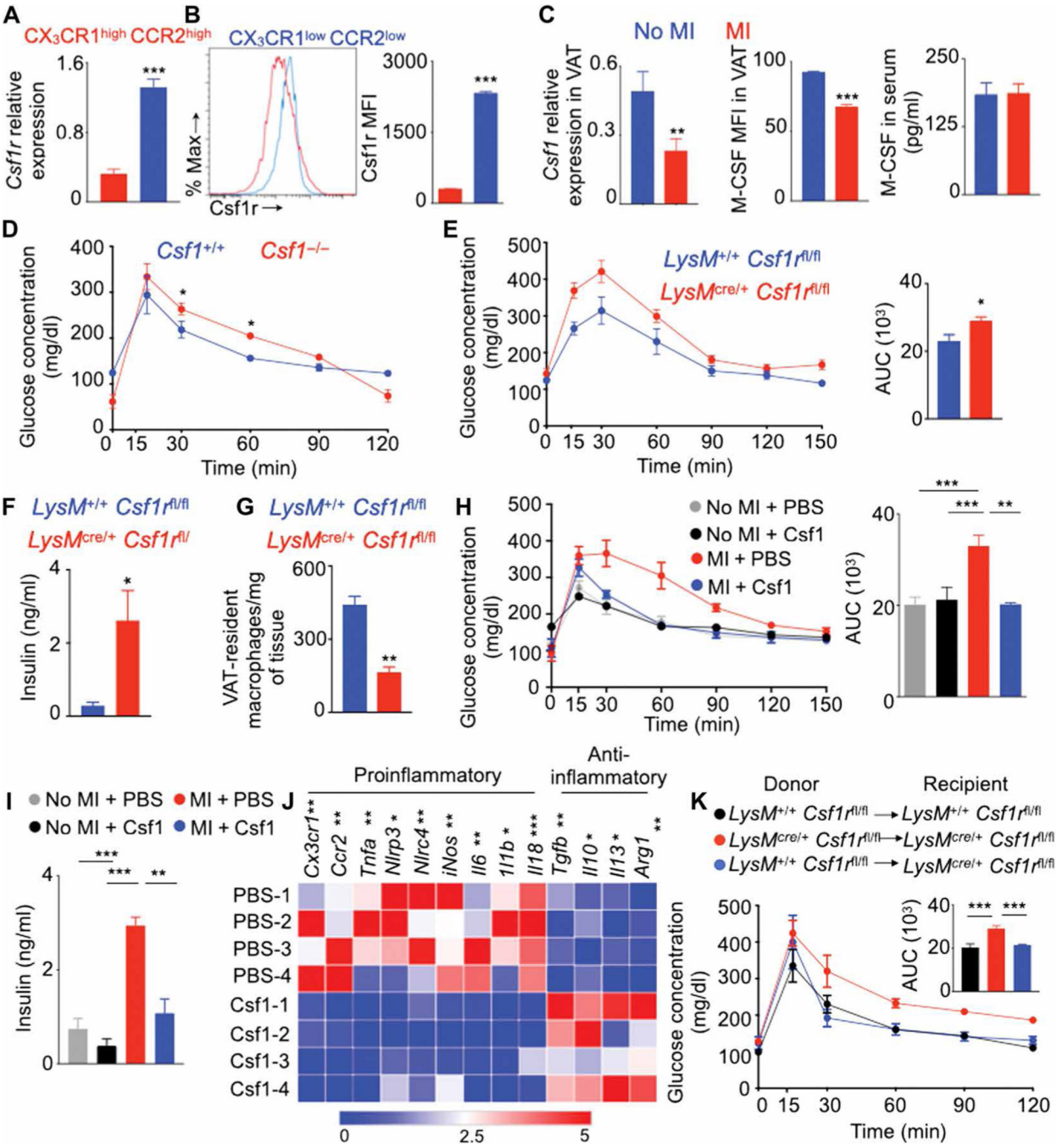

Fig. 7. Diminished Csf1r signaling in macrophages causes insulin resistance after MI.

Quantification of Csf1r in VAT macrophage subsets in the steady state using qPCR (**A**) and flow cytometry (**B**) in lean C57BL/6 mice without MI and *Csf1* in VAT and serum on day 7 after MI in lean C57BL/6 mice (**C**). $n = 3$ to 10 per group. qPCR quantification of *Csf1* relative to *Gapdh* expression is shown. (**D**) GTT in *Csf1*-deficient mice without MI. $n = 3$ to 4 per group. GTT (**E**) ($n = 6$ to 8 per group), fasting insulin concentrations (**F**) ($n = 4$ to 8 per group), and VAT-resident macrophage content (**G**) in lean $LysM^{cre/+}Csf1r^{fl/fl}$ mice on day 7 after MI are shown. $n = 4$ to 6 per group. GTT (**H**) [$n = 12$ for no MI and PBS

(phosphate-buffered saline); $n = 4$ for no MI and M-CSF (macrophage colony-stimulating factor); $n = 7$ for MI and PBS; and $n = 3$ for MI and M-CSF groups], fasting insulin concentrations (**I**) ($n = 5$ per group), and gene array in sorted VAT-resident macrophages (**J**) ($n = 4$ per group) after Csf1 supplementation in lean C57BL/6 mice on day 7 after MI. (**K**) Epididymal adipose tissue was transplanted in different groups of lean mice as shown. MI and GTT were performed on days 10 and 17, respectively, after transplantation. $n = 4$ to 6 per group. Data pooled from two to four independent experiments are shown. MFI, mean fluorescence intensity. Means ± SEM. $*P < 0.05$, $**P < 0.01$, and $***P < 0.001$.

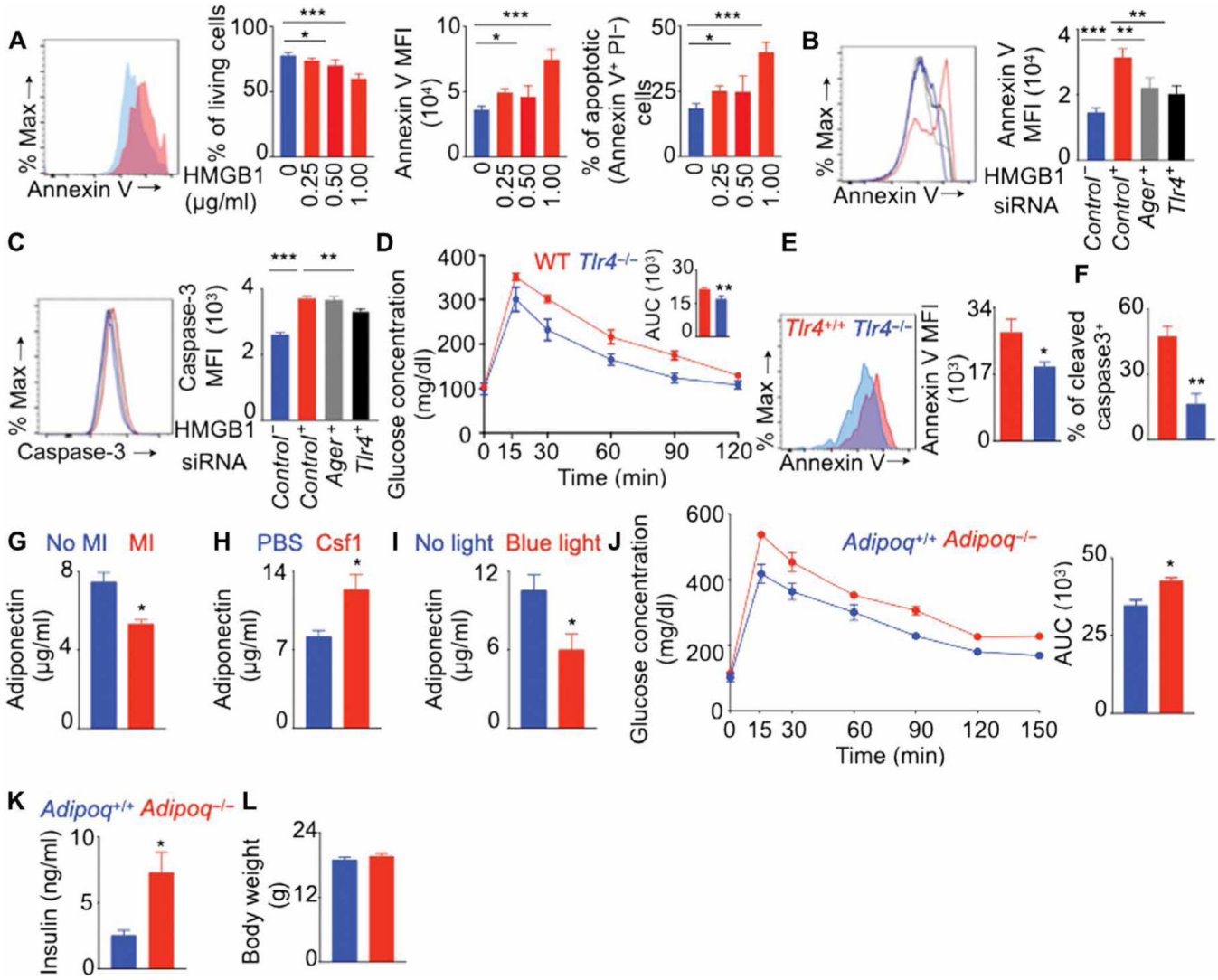

Fig. 8. Decreased adiponectin content after MI induces glucose intolerance.

(**A**) Bone marrow–derived macrophages were cultured with various concentrations of HMGB1. Flow cytometry quantified the frequency of live cells, annexin V expression, and proportions of apoptotic cells. $n = 6$ per group. (**B** and **C**) *Tlr4* and *Ager* were knocked down in BMDM using siRNA, and these cells were cultured with or without HMGB1. $n = 5$ per group. Annexin V (B) and cleaved caspase-3 (C) expression was quantified using flow cytometry. GTT (**D**) and annexin V (**E**) and cleaved caspase-3 (**F**) expression in VAT-resident macrophages were assessed on day 7 after MI in lean $Tlr4^{+/+}$ and $Tlr4^{-/-}$ mice. $n =$ 4 to 5 per group. Adiponectin concentrations were quantified using enzyme-linked immunosorbent assay in the serum of lean C57BL/6 mice on day 7 after MI (**G**) ($n = 6$ to 8 per group), lean C57BL/6 mice on day 7 after MI after Csf1 supplementation (**H**) ($n = 4$ to 5 per group), and lean $LysM^{cre/+}$ $ChR\text{-}2^{fl/fl}$ mice without MI after VAT-resident macrophage depletion with blue light (**I**) ($n = 3$ per group). MI was induced in lean $Adipoq^{+/+}$ and $Adipoq^{-/-}$ mice, and a GTT to assess glucose clearance (**J**); fasting insulin quantification

(**K**); and body weight measurement (**L**) were performed 7 days later. $n = 5$ mice per group. Means ± SEM. $*P < 0.05$, $**P < 0.01$, and $***P < 0.001$.